NASA/CR-97-206273

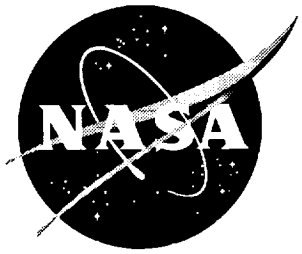

Receptivity of Flat-Plate Boundary Layer in a Non-Uniform Free Stream (Vorticity Normal to the Plate)

M. N. Kogan and M. V. Ustinov

December 1997

The NASA STI Program Office . . . in Profile

Since its founding, NASA has been dedicated to the advancement of aeronautics and space science. The NASA Scientific and Technical Information (STI) Program Office plays a key part in helping NASA maintain this important role.

The NASA STI Program Office is operated by Langley Research Center, the lead center for NASA's scientific and technical information. The NASA STI Program Office provides access to the NASA STI Database, the largest collection of aeronautical and space science STI in the world. The Program Office is also NASA's institutional mechanism for disseminating the results of its research and development activities. These results are published by NASA in the NASA STI Report Series, which includes the following report types:

- TECHNICAL PUBLICATION. Reports of completed research or a major significant phase of research that present the results of NASA programs and include extensive data or theoretical analysis. Includes compilations of significant scientific and technical data and information deemed to be of continuing reference value. NASA counter-part or peer-reviewed formal professional papers, but having less stringent limitations on manuscript length and extent of graphic presentations.

- TECHNICAL MEMORANDUM. Scientific and technical findings that are preliminary or of specialized interest, e.g., quick release reports, working papers, and bibliographies that contain minimal annotation. Does not contain extensive analysis.

- CONTRACTOR REPORT. Scientific and technical findings by NASA-sponsored contractors and grantees.

- CONFERENCE PUBLICATION. Collected papers from scientific and technical conferences, symposia, seminars, or other meetings sponsored or co-sponsored by NASA.

- SPECIAL PUBLICATION. Scientific, technical, or historical information from NASA programs, projects, and missions, often concerned with subjects having substantial public interest.

- TECHNICAL TRANSLATION. English-language translations of foreign scientific and technical material pertinent to NASA's mission.

Specialized services that help round out the STI Program Office's diverse offerings include creating custom thesauri, building customized databases, organizing and publishing research results . . . even providing videos.

For more information about the NASA STI Program Office, see the following:

- Access the NASA STI Program Home Page at ***http://www.sti.nasa.gov***

- Email your question via the Internet to help@sti.nasa.gov

- Fax your question to the NASA Access Help Desk at (301) 621-0134

- Phone the NASA Access Help Desk at (301) 621-0390

- Write to:
  NASA Access Help Desk
  NASA Center for AeroSpace Information
  800 Elkridge Landing Road
  Linthicum Heights, MD 21090-2934

NASA/CR-97-206273

Receptivity of Flat-Plate Boundary Layer in a Non-Uniform Free Stream (Vorticity Normal to the Plate)

M. N. Kogan and M. V. Ustinov
Central Aerohydrodynamics Institute (TsAGI), Zhukovski, Moscow Region, Russia

National Aeronautics and
Space Administration

Langley Research Center
Hampton, Virginia 23681-2199

Prepared for Langley Research Center
under Cooperative Agreement NCC1-241

December 1997

Available from the following:

NASA Center for AeroSpace Information (CASI)
800 Elkridge Landing Road
Linthicum Heights, MD 21090-2934
(301) 621-0390

National Technical Information Service (NTIS)
5285 Port Royal Road
Springfield, VA 22161-2171
(703) 487-4650

Abstract

The reported work is devoted to study of free-stream vorticity normal to leading edge interaction with boundary layer over plate and resulting flow distortion influence on laminar-turbulent transition. In experiments made the wake behind the vertically stretched wire was used as a source of vortical disturbances and it's effect on the boundary layer over the horisontally mounted plate with various leading edge shapes was investigated. The purpose of experiments was to check the predictions of theoretical works of M.E. Goldstein et. al. [4-6]. This theory shows that small free-stream inhomogeneity interacting with leading edge produces considerable distortion of boundary layer flow. In general, results obtained confirms predictions of Goldstein's theory, i.e. the amplification of steady vortical disturbances in boundary layer caused by vortex lines streaching was observed. However, experimental results fully coincides with predictions of theory for large Reynolds number, relatively sharp leading edge and small disturbances. For large enough disturbances the flow distortion caused by symmetric wake unexpectedly becomes antisymmetric in spanwise direction. If the leading edge is too blunt (semicircular) the maximal distortion takes place immediately at the nose and no further amplification was observed. All these conditions and results are beyond the scope of Goldstein's theory. Another surprising result is the absence of laminar-turbulent transition in the boundary layer strongly distorted by wake. Theory of spanwise modulated flow stability developed in theoretical part of report explains this effect.

1. Introduction

Recent progress in both the linear and nonlinear aspects of stability theory has highlighted the importance of receptivity problem [1]. One of the most unclear part of receptivity studies is the receptivity of boundary-layer flow to vortical disturbances. Some experimental [2] and theoretical [3] results permits to propose that quasi-steady outer-flow vortical disturbances may trigger by-pass transition. For this reason the experimental and theoretical study of vortex-boundary layer interaction is an actual task. In present work such interaction is investigated for the vorticity normal to the leading edge. The interest to this type of vortical disturbances arises from the theoretical works of M.E. Goldstein et. al. [4-6], where it was shown that small sinusoidal variation of upstream velocity along the spanwise direction can produce significant variations in the boundary-layer profile.

In experimental part of this work (section 2) such non-uniform flow interaction with boundary layer over flat plate with nose of various shape was investigated. The non-uniform flow was produced by laminar wake behind the wire placed normal to the plate upstream of the leading edge. Theoretical part of the work

(section 3) is devoted to stability study of boundary layer flow with spanwise modulated velocity profile similar to that produced by outer-flow vorticity.

2. Experimental study of wake-boundary layer interaction for different leading edge shapes

2.1. Experimental setup and equipment

The experiment was performed in a low-turbulence direct-flow wind tunnel T-36 I of Central Aerohydrodynamics institute (TsAGI). The test section is 2.6 m long, 0.5 m wide and 0.35 m high, and is preceded by 18:1 contraction. The free-stream turbulence level in the test section is 0.06%, measured in the band 5-1500 Hz at velocities grater then $5m/s$. Wind tunnel and flow characteristics in test section are described in more details in previous report.

The general outline of experimental setup is shown in Figure 1 a. Interaction of wake from vertically stretched wire with the boundary layer over the horizontally mounted plate was studied. Two plates with semi-elliptical leading edges of aspect ratious 4:1 and 1:1 were used. These plates of 1810 mm long, 500 mm wide and 20 mm thick were made from Plexiglas and had drains for static pressure distribution measurements. To control the stagnation point position over nose two flaps mounted above the plate near its trailing edge were used. The wire was stretched at the holder moving horizontally with steps 0.1 mm. Streamwise velocity component in boundary layer was measured with a DISA 55M01 anemometer and a single hot wire probe made of a gold plated tungsten with a wire diameter $5\mu m$ and a sensitive length of 1 mm. The probe was mounted on a carriage and was transversed in streamwise and vertical directions. The accuracy of probe movement in vertical direction was 0.1 mm. Instead of probe movement in spanwise direction the horizontal transmission of the wire was used. Coordinate system and general designations used are shown in Figure 1 b, c.

2.2. Undisturbed flow characteristics

Interaction of wake with boundary layer over flat plate was studied for two semi-elliptical leading edges with aspect ratious 4:1 and 1:1 and two free stream velocities 5 m/s and 17 m/s. So "blunt" plate nose forms were chosen to attain more strong and distinct wake/boundary layer interaction effects. For relatively sharp leading edge 4:1 the nearly symmetrical flow over the nose was reached. This is illustrated by Figure 2 a where the velocity distribution over upper and lower sides of nose computed from static pressure measured is shown. For symmetric flow over blunt semicircular nose with aspect ratio 1:1, the local separation bubble located near nose-plate mating occurs. To eliminate the separation bubble the attachment line was moved to upper part of nose and flow becomes substantially asymmetric. The velocity distribution over nose in this case is shown in Figure

2 *b*. From this figure one can see that velocities in first two points on the upper surface are approximately the same, especially for $u_\infty = 5m/s$. So, stagnation point is located between two first drains i.e. at y between 2 and 4 mm. Special efforts were made to achieve the similar flow over the leading edge for two free stream velocities 5 and 17 m/s. Figure 2 demonstrates satisfactory coincidence of nondimensional velocity distributions measured at these two flow velocities for both leading edges. On working upper surface the difference between them is less then 5%.

Velocity distributions along the plane parts of models, measured for $u_\infty = 5m/s$ by hot wire probe outside the boundary layer (at $y = 40mm$) are plotted in Figure 3. Similar results for $u_\infty = 17m/s$ are not shown because they coincides with data for $u_\infty = 5m/s$ within the accuracy of measurements ($\sim 0.3\%$). For sharp nose (1:4) there exist a slight negative pressure gradient along x and pressure gradient is slightly positive for blunt nose (1:1). All these gradient are very small with velocity varies by 1% over the length of 1 m.

Velocity profiles in the boundary layer at different distances x from the leading edge for all combinations of u_∞ and nose shapes are shown in Figures 4-7 (see captions for these figures). Near the leading edge ($x = 20$ and 40 mm) the profiles have maxima at the joint of boundary layer and inviscid flow. The velocity at these maxima (shown by open symbols in figure 2) closely coincides with velocity obtained from static pressure measurements. Far from leading edge velocity profiles tends to Blasius profile for flat-plate boundary layer.

For the plate with sharp nose (1:4) the velocity pulsations in the boundary layer were less then 0.1% u_∞ over all plate length for both free stream velocities. The similar velocity pulsations level was observed in the boundary layer at the plate with blunt nose (1:1) for $u_\infty = 5m/s$. At these regimes the boundary layer flow was fully laminar. Laminar -turbulent transition occurs in a boundary layer over the blunt nose plate at $u_\infty = 17m/s$. This is illustrated by Figure 8, where the $x-$distribution of mean flow velocity $\overline{u} = u/u_\infty$ and r.m.s. pulsations $\overline{u}' = u'/u_\infty$ measured at fixed $y = 0.3mm$ are shown. For this flow configuration the boundary layer remains laminar till $x = 200mm$ and transition occurs at $x \sim 450mm$. Two factors may cause the transition: positive pressure gradient and amplification of outer flow pulsations at the blunt nose.

2.3. Wake-boundary layer interaction

As was mentioned above, the purpose of reported work is investigation of laminar wake interaction with flat plate boundary layer. It's well known that steady laminar flow in the wake behind a cylinder exists if Reynolds number $R_d = u_\infty d/\nu$ is less then 40-50 [8]. Unfortunately, the laminar wakes are too narrow for well-measured velocity deficit values. So, it is difficult to meet the conditions of Goldstein's theoretical scheme, where the wake width $2L$ should be many times higher then boundary layer thickness. Moreover, the Reynolds number associated

with laminar wake $\sigma = 2u_0L/\nu \sim R_d$ is small with respect to Reynolds number of typical outer flow disturbances $\sigma = 70$ in Kendall's experiment [9] (see also [6]). In order to enhance the wake Reynolds number in experiment, the wake behind a wire in regime of Karman vortex sheet was used. Up to $R_d = 200$ this vortex sheet remains two-dimensional [8]. This sheet decays gradually with distance and for $x \geq 100d$ it becomes indistinguishable from background pulsations in the wake [8]. Pulsations in such decayed Karman vortex sheet are about 1/20 of it's velocity deficit. It is more then in laminar wake, but it is sufficiently less then in turbulent one.

In the reported work three wakes were used as a sources of upstream flow inhomogeneity. One of them is steady laminar wake behind a wire of $d = 0.09\ mm$ in a flow with $u_\infty = 5m/s$. The Reynolds number of this wake is $R_d = 31$ and velocity pulsations within it are the same as in the free stream. Two other wakes are the decayed Karman sheets with $R_d \simeq 100$: the wake behind a wire of $d = 0.09\ mm$ in a flow with $u_\infty = 17m/s$ and a wake produced by wire of $d = 0.3\ mm$ in a flow with $u_\infty = 5m/s$. Velocity deficits $\overline{u_0} = u_0/u_\infty$, half-widths L, and maximal over z pulsations in these two wakes as functions of distance from wire are plotted in Figures 9 and 10 respectively. Characteristics of steady laminar wake are well described theoretically as

$$\frac{u_0}{u_\infty} = B\sqrt{\frac{d}{x}} \quad \frac{L}{d} = A\sqrt{\frac{x}{d}} \quad A = 2\sqrt{\frac{\ln 2}{R_d}} \quad B = \frac{C_x}{4}\sqrt{\frac{R_d}{\pi}}$$

where C_x is drag coefficient of the wire. From experimental data it was found that $B = 1.35$.

Interaction of these three wakes with the boundary layer over the plate with two noses were studied for different distances from wire to leading edge. All flow configurations (diameter of wire, velocity, distance from wire to the leading edge, shape of the leading edge) tested and characteristics of wakes at the leading edge locations in these configurations are listed in the Table. Interacting with leading edge, the wake produces two types of flow distortion in boundary layer. Symmetric distortion generally observed if the wake is sufficiently weak. An example of such distortion observed in flow configuration 3 is presented in Figure 11. This figure shows the spanwise distributions of mean velocity in boundary layer $\overline{u} = u/u_\infty$ measured at different distances from the leading edge. The distance from the wall where these distributions were measured varies with x and corresponds to $\overline{u} \sim 0.5$. When the wire was moved toward the leading edge at $x_w = 40mm$ (configuration 1 in Table), the flow distortion in boundary layer becomes antisymmetric. This is demonstrated in Figure 12, where the similar velocity profiles for this flow configuration are plotted. There are two possible antisymmetric regimes: the "left" regime with maximum of velocity at the left side and the right one with maximum at the right side. Both of these regimes were observed and they change each other randomly when the wind tunnel was

stopped and started again. An attempt to fix the flow distortion orientation by means of getting wire out of blunt by about 5^0 was unsuccessful because of both "left" and "right" regimes were observed with non-vertical wire too. The only effect of wire inclination was slight loss of left-right symmetry with one of regimes ("left" or "right") becomes more pronounced. For definiteness, in all Figures dealing with antisymmetric flow distortion the left regime is shown. Transformation of outer symmetric wake flow into the antisymmetric flow in the boundary layer is illustrated by Figure 13 where the streamwise velocity distribution measured in section $x = 150mm$ in configuration 1 is shown. The gradual transition of antisymmetric regime into symmetric with x_w growth is demonstrated by Figure14 showing the velocity profiles in section $x = 150mm$ for $x_w = 40,\ 150$ and $250mm$.

To explain a phenomenon of antisymmetric regime formation let's consider a conceptual scheme of wake-leading edge interaction shown in Figure 15. The wake may be considered as a pair of counterrotational vortex sheets. Stretching of these sheets vortex lines around the nose produce a pair of counterrotational streamwise vortices at the plate surface. The streamwise vorticity leads to a perturbation of the streamwise boundary layer velocity. In symmetric regime, the lifting of fluid between the vortices causes the diminishing of the streamwise velocity, whereas at the periphery of them the downwards outer flow leads to growth in the boundary layer velocity. The local maximum of velocity in the middle of the wake in this regime may be caused by small-size secondary vortices originating between the main vortices as shown in Figure 15 *b*.

It's well known that a pair of counterrotational streamwise vortices in a free stream exhibits the so-called Crow instability [7]. This instability manifests in twisting of vortices in a spiral manner. If similar type of instability exists for near-wall vortices it will lead to lifting of one vortex as shown in Figure 15 *c*. The remaining vortex will produce an antisymmetric flow distortion in the boundary layer. If the symmetric regime is stable it is the only possible solution of wake-boundary layer interaction problem. When it becomes unstable, the bifurcation of solution occurs and new stable antisymmetric solution observed in experiment appears. Contrary to unbounded stream where the Crow instability occurs for all vortex strengths, the wall should stabilize the vortex pair. The instability should occur only if the vortices are strong enough to lift each other. In accordance with rapid distortion theory, the streamwise vorticity is proportional to initial vertical vorticity in the wake which may be estimated as u_0/L. The instability should exist if this vorticity is large with respect to some characteristic velocity gradient in a flow around the nose. If we suppose the inviscid nature of instability, this gradient should be u_∞/D, and the non-dimensional stability criterion $K = \frac{u_0}{L}\frac{D}{u_\infty}$ can be constructed. If the instability related with vortices/boundary layer interaction is expected, the vorticity should be related to velocity gradient in boundary layer over nose. In this case, the stability criterion becomes $K_\nu =$

$\frac{u_0}{L}\frac{\delta}{u_\infty}$, where $\delta = \left(\frac{r\nu}{u_\infty}\right)^{1/2}$ is the boundary layer thickness in the stagnation point and r - the radius of the nose. Both criteria for all configurations tested are given in Table. Comparison of two criteria shows that transition of a symmetric flow into antisymmetric one some better correlates with inviscid criterion K. Boundary layer flow is symmetric for $K \leq 1$ and becomes antisymmetric for $K \geq 2$. Symmetric distortion occurs when $K \geq 2$ in configurations 7 and 8 only. For these flow configurations the wake width is approximately equal to boundary layer thickness and wake-boundary layer interaction is fully viscous. In any case this correlation shows the significant role of inviscid processes in symmetry/antisymmetry transformation.

There are many parameters effecting on wake-boundary layer interaction. Three of them describing the ongoing wake R_d , K and K_ν were already introduced. Another significant parameter responsible to relative boundary layer thickness is unit Reynolds number $R_1 = u_\infty 1/\nu$. To simplify the analysis of these parameters influence on phenomenon under consideration, let's introduce the amplification coefficient describing the boundary layer flow response to initial vortical disturbances. This coefficient r is the ratio of boundary layer flow distortion Δu_b at a given section x and the velocity deficit in ongoing wake near the leading edge u_{0le}, that is $r = \Delta u_b / u_{0le}$. The distortion Δu_b is determined as a difference between the maximum and minimum of velocity distribution over span measured for y corresponding to $\overline{u} \sim 0.5 - 0.7$. Distortion determined by this way is close to it's maximum over section $x = const$. The amplification coefficients as functions of x computed for different flow configurations are shown in Figure 16. From these results one can see, that the influence of unit Reynolds number on amplification coefficient is considerably stronger then the effect of other factors. For large unit Reynolds number regimes 1,3,9,10,11 with $u_\infty = 17m/s$ and $R_1 = 1.17 \cdot 10^6$ the amplification coefficients are an order of 10, whereas for regimes 4,5,8 with $u_\infty = 5m/s$ and $R_1 = 3.45 \cdot 10^5$ this coefficient is not larger then 2.

The second in significance factor is the shape of nose, with amplification coefficients for blunt nose (1:1) is an approximately two times grater then for sharp nose (1:4). At the plate with blunt nose the maximal flow distortion is reached immediately at the leading edge and perturbations decays rapidly with x. For the sharp 1:4 nose the flow distortion reaches it's maximum at the noticeable distance $x \sim 100 - 150mm$ from leading edge. It is interesting to note, that antisymmetric disturbances (configurations 1, 4) decay more slowly then symmetric ones (configurations 3, 5,8).

Maximal over z velocity pulsations in boundary layer distorted by wake measured at y corresponding to $\overline{u} = 0.5 - 0.7$ for some of configurations tested are shown in Figure 17. Laminar-turbulent transition occurred only over plate with 1:1 nose at $u_\infty = 17m/s$ (configurations 9,10,11). In these configurations the extremely large pulsations $\overline{u'} \sim 6 - 10\%$ were observed at the first near-nose

section $x = 20mm$. It is not surprising, that such high pulsations trigger the laminar-turbulent transition at small distance $\sim 150-250mm$ from leading edge. Unfortunately, for these flow configurations (9,10,11) the wake-boundary layer interaction can not be considered as laminar, i.e. the effect of pulsations on mean flow development is significant over whole plate surface. The possible reason of pulsations origination near leading edge may be local flow separation provocated by wake. Really, the flow distortion in section $x = 20mm$ for configurations 9 and 11 is very strong (see Figures 18 *a* and 19 *a*) and they may correspond to separated flow in boundary layer. For all other configurations the pulsations level did not exceeds 2% of outer flow velocity at least for $x \leq 700mm$. Such small pulsations could not have any influence on steady flow distortion development, so wake-boundary layer interaction may be considered as fully laminar. It's interesting to note, that remarkable flow distortion in boundary layer observed in configurations 1-3 ($\Delta u_b/u_\infty \sim 0.3 - 0.4$) did not lead to flow turbulization. Possible explanations of this phenomenon see in section 3.

Figure 18 shows the spanwise distributions of $\overline{u}$ measured at $x = 20$ or 40 and 150 in flow configurations 9, 1, and 4 where antisymmetric distortion were observed. The shapes of this distributions are almost the same and does not depends on nose shape, R_1, R_d and other parameters. Similar distributions for configurations 11, 3, 5 and 8 with symmetric flow distortion are shown in Figure 19. Two distinct types of velocity distribution are seen in this Figure. Profiles of first type with maximum at the centre were observed under high unit Reynolds number (configurations 3 and 11). If the unit Reynolds number is small (configurations 5 and 8) this maximum disappeared. The central maximum in low unit Reynolds number flows appears only in velocity profiles measured close to the wall. Such profiles may be found in figure 20 showing the velocity distribution at $x = 100\ mm$ for flow configuration 5.

Distributions of boundary layer flow distortion Δu_b over y measured in section $x = 150mm$ in flow configuration 1and in section $x = 100mm$ in flow configurations 5 and 8 are plotted in Figure 21. For convenience, this distortions are normalized by their values in outer flow measured at $y = 40mm$ (deficit of the wake u_0) and vertical coordinate is referred to undisturbed boundary layer displacement thickness δ^*. For comparison , the profile of velocity pulsations measured in boundary layer under enhanced outer flow turbulence level by Kendall [9] is plotted in this figure too. Results of [9] were normalized to fit maxima of pulsations and flow distortion in configuration 1. Figure 21 shows good coincidence of flow distortion profile measured in antisymmetric regime for high unit Reynolds number configuration 1 with profile of pulsations in [9]. Similar coincidence also was demonstrated for symmetric flow distortion computed in frame of Goldstein's theory [6]. So, one may suppose that both symmetric and antisymmetric regimes of flow distortion take place when free-stream turbulence interacts with leading edge.

3. Stability of boundary layer with steady inhomogeneity of velocity profile

In this section the stability of boundary layer flow with steady spanwise modulation of velocity profile is studied theoretically. Such modulation is a model of a streaky structure originating in the boundary layer subjected to free-stream turbulence. The non-uniform flow in boundary layer produced by wake is another example of modulated flow. It's well-known that transition is not caused directly by steady flow distortion, but it's initiated by the growth of high-frequency travelling waves. For this reason, the stability studies of modulated flows are necessary for understanding of transition caused by outer flow turbulence. In contrast to generalized Rayleigh's equation approach used in [6], the stability analysis is based on more general linearized Navier-Stokes equations.

3.1. Problem formulation

Consider the stability of boundary layer flow with steady variations of velocity profile in spanwise direction. We'll use the coordinate system introduced in section 2 with lengths scaled with averaged over span boundary layer displacement thickness δ^*. Basic flow $\mathbf{V}_0(y,z)$ is considered to be spanwise-periodic with period T_z and homogeneous in streamwise direction. We present this flow in form of Fourier series

$$\mathbf{V}_0 = \{U_0(y),0,0\} + \mathbf{V}_i \quad \mathbf{V}_i = \sum_{n=-N}^{N} \mathbf{V}_{0n} e^{in\beta z} \qquad \mathbf{V}_i = \{u_i, v_i, w_i\} \tag{3.1}$$

where $U_0(y)$ - Blasius flow profile, $\mathbf{V}_i$ - flow inhomogeneity, $\beta = 2\pi/T_z$.

There are two general types of unstable disturbances in periodic flows: the disturbances of the same period as the basic flow (fundamental disturbances) and subharmonic ones. Disturbances of both types will be sought in common form

$$\mathbf{V}_p = \left[\sum_{n=-N}^{N} \mathbf{V}_n(z) e^{in\frac{\beta}{2}z}\right] e^{i(\alpha x - \omega t)} \quad \mathbf{V}_p = \{u,v,w\} \tag{3.2}$$

We'll consider the temporal stability i.e. complex ω corresponding to real α will be sought.

Substitution of complete flow-field $\mathbf{V} = \mathbf{V}_0 + \epsilon\mathbf{V}_p$ into Navier-Stokes equations and linearization in ϵ gives an eigenvalue problem for ω

$$-i\omega\mathbf{L}_2 \circ \mathbf{V}_p = \mathbf{L}_1 \circ \mathbf{V}_p \tag{3.3}$$

where $\mathbf{L}_1$ and $\mathbf{L}_2$ are linear operators including derivatives with respect to y. Discretization of (3.3) in y yields the eigenvalue problem for matrix

$$(\mathbf{A} - i\omega\mathbf{E})\mathbf{F} = 0 \qquad \mathbf{A} = \mathbf{D}^{-1}\widetilde{\mathbf{A}} \tag{3.4}$$

Here vector $\mathbf{F}$ includes discrete representation of disturbances and matrixes $\widetilde{\mathbf{A}}$ and $\mathbf{D}$ corresponds to operators $\mathbf{L}_1$ and $\mathbf{L}_2$.

3.2. Numerical method

In all works where stability of periodic flows is studied the matrixes $\widetilde{\mathbf{A}}$ and $\mathbf{D}$ were determined and eigenvalue problem (3.4) is solved. Here we'll introduce an alternative approach to stability of complex geometry flows which is based on algorithm for Navier-Stokes equations solution. This approach makes us possible to study the stability of any periodic flow using a code for DNS of periodic flows. In all of these codes the flow field is presented in form of two-dimensional Fourier series in (x, z) plane. If we fix a part of harmonics representing basic flow, then remaining harmonics will describe the evolution of disturbances. If the amplitude of disturbances is small enough, it's evolution is described by linearized (near the basic flow) Navier-Stokes equations. These equations may be written in form similar to (3.3)

$$\frac{\partial}{\partial t}(\mathbf{L}_2 \circ \mathbf{V}'_p) = \mathbf{L}_1 \circ \mathbf{V}'_p$$

where $\mathbf{L}_1$ and $\mathbf{L}_2$ are the same as in (3.3). All codes for DNS solve the discrete version of these equations of form

$$\frac{\partial}{\partial t}\mathbf{G} = \mathbf{A}\mathbf{G}$$

Here $\mathbf{A}$ is the same matrix as in (3.4) and $\mathbf{G}$ contains discrete representation of disturbances. If the finite-difference scheme used in DNS code is known, the matrix $\mathbf{A}$ may be easily related with matrix of transition $\mathbf{B}$. The former matrix describes the evolution of disturbances over one time step τ and relates disturbances at time t, $\mathbf{G}^k$ and at time $t + \tau$, $\mathbf{G}$ as

$$\mathbf{G} = \mathbf{B}\mathbf{G}^k$$

Transition matrix may be directly computed using DNS code. For Crank-Nicholson scheme used in our code, matrix $\mathbf{B}$ is related with $\mathbf{A}$ as

$$\mathbf{B} = \left[\mathbf{E} - \frac{\tau}{2}\mathbf{A}\right]^{-1} \times \left[\mathbf{E} + \frac{\tau}{2}\mathbf{A}\right]$$

It is easy to prove that matrixes $\mathbf{A}$ and $\mathbf{B}$ have the same eigenvectors, and eigenvalues of $\mathbf{B}$, μ_j are related with eigenvalues of $\mathbf{A}$, λ_j as

$$\mu_j = \frac{1 + \frac{\tau}{2}\lambda_j}{1 - \frac{\tau}{2}\lambda_j}$$

So eigenvalues ω_j of stability problem may be obtained from μ_j as

$$\omega_j = -\frac{2i}{\tau}\frac{1 - \mu_j}{1 + \mu_j}$$

The form of disturbances corresponding to ω_j is determined by eigenvector of $\mathbf{B}$ associated with μ_j.

The method described here was tested by means of computation of Blasius flow stability and the secondary instability of finite-amplitude TS wave. The results were in excellent agreement with those of traditional methods.

3.3. Results

Stability of Blasius boundary layer with $R = u_\infty \delta^* / \upsilon = 1000$ distorted by harmonic velocity modulation or by localized flow inhomogeneity were studied. The first flow is a model of periodic streaky structure observed under enhanced outer flow turbulence level, the second one is a model of the single streak or distortion produced by wake studied in section 2. In both flows inhomogeneity velocity vector $\mathbf{V}_i$ had only streamwise component u_i of form

$$u_i = af(y)g(z)$$

where a is an amplitude, functions $f(y)$ and $g(z)$ defines vertical and spanwise distribution of flow inhomogeneity. Vertical distribution for both flows was

$$f(y) = \frac{\exp(-\frac{(y-y_0)^2}{\Delta^2}) - \exp(-\frac{(y+y_0)^2}{\Delta^2})}{\max\limits_y \left[\exp(-\frac{(y-y_0)^2}{\Delta^2}) - \exp(-\frac{(y+y_0)^2}{\Delta^2})\right]} \tag{3.5}$$

with parameters $\Delta = 1.2$ and $y = 1.4$ chosen for coincidence with profile of low-frequency pulsations measured in boundary layer subjected to free-stream turbulence [9]. This profile is plotted by solid line in Figure 22 *a* together with profile of velocity pulsations from [9] shown by points. For the harmonic inhomogeneity spanwise distribution was

$$g(z) = \cos \beta z$$

whereas for localized inhomogeneity it was represented as

$$g(z) = \frac{1-q}{2}\left[1 + (1+q)\sum_{n=1}^{N} q^n \cos n\beta z\right] \qquad q < 1 \tag{3.6}$$

The last function with $q = 0.63$ shown in Figure 22 *b* has a narrow maximum within $z = 0$ and vanishes over the remaindind part of period.

Due to basic flow symmetry, the disturbances may be symmetric or antisymmetric, i.e. the streamwise velocity of disturbances may be even or odd function of z. As was mentioned above, the disturbances of both these types may have fundamental or subharmonic period. So, there exist four types of unstable modes. Figure 23 shows the spanwise distribution of streamwise velocity $Re(u)$ and amplitudes of pulsations $|u|$ for all these modes computed for harmonically

modulated flow with $a = -0.3$, $\alpha = 0.25$, $\beta = 0.6$. Symmetric and antisymmetric fundamental modes are shown in Figure 23 *a* and *b*, whereas Figure 23 *c* and *d* shows symmetric and antisymmetric subharmonic disturbances. For symmetric modes $|u|$ is largest at the minimums of basic flow velocity u_i, whereas maximal pulsations of antisymmetric modes coincides with maxima of gradients $|\partial u_i/\partial z|$. The phase velocity of symmetric modes coincides with TS wave velocity, but antisymmetric disturbances propagate faster with $c = Re(\omega)/\alpha = 0.6$. Further computations reveals that the subharmonic mode is the most unstable one among the antisymmetric disturbances and the fundamental mode is the most amplified symmetric disturbance. So, only subharmonic antisymmetric and fundamental symmetric modes will be considered later. For brevity, these modes will be named as antisymmetric and symmetric ones.

Growth rates $\theta = Im(\omega)$ of symmetric and antisymmetric modes as functions of amplitude a and spanwise wavenumber β are shown in Figures 24 and 25 respectively. These results were computed for $\alpha = 0.25$; amplitude dependance of θ corresponds to $\beta = 0.6$, and $\theta(\beta)$ corresponds to $a = 0.3$. Growth rates of all modes increase with amplitude growth. For small amplitudes of flow inhomogeneity the symmetric modes are the most unstable, whereas antisymmetric disturbances becomes the most amplified for large amplitudes $a \geq 0.3$. The β- dependences of growth rates are different for symmetric and antisymmetric modes. Growth rates of symmetric modes are maximal for $\beta = 0$ and gradually decrease with growth of β. Amplification rates of antisymmetric disturbances initially increases with β growth, then reaches maximum at $\beta = 0.6$ and falls off. This result contradicts with conclusion of [10] about growth rate of these modes proportionality to $|\partial u_i/\partial z|$.

Figure 26 shows the growth rates of symmetric and antisymmetric modes as functions of reduced frequency $F = 10^6\omega/R$ computed in flow with $a = -0.3$ and $\beta = 0.6$. Both symmetric and antisymmetric disturbances amplify much rapidly then TS waves. The growth rates of these two types of modes are comparable, with symmetric modes are the most unstable at large frequency, whereas the antisymmetric modes are the most amplified low-frequency disturbances. Instability occurs in wide frequency range $20 \leq F \leq 220$ with maximal growth rate achieves at $F = 150$. Disturbances in the same frequency range amplified in the boundary layer flow with embedded streamwise vortices in experiment [10].

Stability localized inhomogeneity flow (3.6) with positive and negative amplitudes $a = \pm 0.3$ was studied in order to reveal the influence of width of inhomogeneity region on flow stability. For this purpose the stability of flow (3.6) with $q = 0.63$ and various β with respect to symmetric modes was computed. The results shown in Figure 27 demonstrates that the flow with high-speed streak has almost the same stability characteristics as homogeneous Blasius flow. In flow with low-speed streak the growth rates of disturbances remains the same as in Blasius flow if $\beta \geq 0.2$. The instability in this flow becomes remarkable only if $\beta \leq 0.2$, with growth rate of disturbances increases with β diminishing.

It means that single thin streak does not destabilize flow in spite of inflexible velocity profile within it. The remarkable instability in this streak occurs only if it's width exceeds a threshold value $L^* \sim 7\delta^*$. This fact explains the absence of transition in boundary layer distorted by wake studied in section 2. Really, in all flow configurations tested, the width of distorted part of boundary layer did not exceeds the threshold value predicted by theory. It's interesting to note that the harmonic modulation of small spanwise period $T_z \leq L^*$ ($\beta \geq 1$) leads to remarkable instability (see Figure 25). So, the periodically placed streaks are more dangerous that equal sole streak.

4. Discussion and conclusions.

The purpose of experimental investigation made is to check the predictions of Goldstein's theory [4-6] describing the interaction of non-uniform flow with boundary layer over the plate. The asymptotic variant of this theory [4] valid for $\sigma \simeq R_d \to \infty$ and R_1 sufficiently large predicts the linear with x growth of boundary layer distortion at linear stage of it's development. Further, when distortion reaches value ~ 1 the non-linear distortion development leads to singularity at finite distance from leading edge. The modified theory valid for finite R_d [6] predicts initial linear growth of distortion, then it reaches maximum and rapidly falls out due to the action of viscosity. Obviously, the theory predicts only symmetric regime i.e. symmetric upstream flow disturbances transforms into symmetric boundary layer distortion.

Among all flow configurations tested only distortion observed in configuration 3 (nose 1:4, $u_\infty = 17m/s$, $x_w = 250mm$, $d = 0.09$) entirely coincides with predictions of Goldstein's theory. For all low unit Reynolds number configurations the distortion began to decay immediately from the leading edge. The discrepancy between theory and experiment in this case may be caused by relatively large boundary layer thickness in our experiment. For these configurations the boundary layer thickness δ^* at $x \sim 100mm$ was only 1.5-3 times smaller then half width of wake L. In theory L/δ^* ratio should be large for viscosity did not effect on vortex lines deformation.

For blunt nose (1:1) the distortion reaches an extremely high value of $\sim 0.6u_\infty$ immediately on leading edge. In this case the stretching of vortex lines in the vicinity of nose is too strong or the near-separation boundary layer near the nose is very sensitive to outer flow streamwise vorticity. The development of such strong disturbances in non-Blasius boundary layer is beyond the scope of Goldstein's theory.

The theoretical part of the work is devoted to study of spanwise-modulated flow stability. This flow is a model of streaks found in experiment of Kendall [9] at high free-stream turbulence level. It was shown that one isolated streak is more stable then periodically placed streaks of the same shape. The isolated streak

does not destabilize flow at all if it is narrowly then threshold value of $\sim 7\delta^*$. This fact explains the absence of transition in most of configuration tested, where the width of distorted part of flow was less then this threshold value.

The main results of the work are:

1. Demonstration of steady vortical disturbances amplification in the boundary layer in a qualitative agreement with Goldstein's theory.

2. Detection of antisymmetric boundary layer flow distortion caused by ongoing symmetric wake.

3. Drastic influence of nose shape and unit Reynolds number on wake-boundary layer interaction.

4. Weak influence of flow distortion in single narrow streak on laminar-turbulent transition. Theoretical explanation of this phenomenon.

References

[1] Bushnell, D. Viscous drag reduction in aeronautics, *ICAS'94 Proceedings, Anaheim, USA, September 18-23, 1993*

[2] Breuer, K.S. & Landahl, M.T. The evolution of localized disturbances in a laminar boundary layer. Part 2. Strong disturbances, *J. Fluid Mech.*,1990,v. 220, 595-621.

[3] Butler K. M.O.& Farrel B.F. Three-dimensional optimal perturbations in viscous shear flows, *Phys. Fluids, 1992, A,* **4**, 1637-1650.

[4] Goldstein M.E., Leib S.I., Couley S.J. Distortion of a flat plate boundary layer by free-stream vorticity normal to the plate. *J. Fluid Mech.,1992,* v. 237, p.231-260.

[5] Goldstein M.E., Leib S.I. A note on the distortion of flat-plate boundary layer by free-stream vorticity normal to the plate. *J. Fluid Mech.,1993,* v. 248, p.531-541.

[6] Goldstein M.E. On the environmental realizability of algebraically growing disturbances and their relation to Klebanoff modes. *Presented at Florida State University International Symposium on Theoretical and Computational Fluid Dynamics in honor of Sir James Lighthill.*

[7] Crow S.C. Stability theory for a pair of trailing vortices. *AIAA paper* 90-1504, 1990

[8] Mansy H.,Yang P.M., Williams D.R. Quantitative measurements of three-dimensional structures in the wake of a circular cylinder. *J. Fluid Mech.*, 1994, V.270, pp.277-296.

[9] Kendall J.M. Experimental study of disturbances produced in a pre-transitional laminar boundary layer by weak free-stream turbulence. *AIAA paper* 85-1695, 1985

[10] Bakchinov, A.A., Grek, G.R., Klingmann, B.G.B., Kozlov, V.V. (1995) Transition experiments in a boundary layer with embedded streamwise vortices, *Phys. Fluids,* v. **7**, pp. 820-832.

Table

number of configu ration	nose	U_∞	d [mm]	x_w [mm]	u_o/u_∞	L [mm]	R_d	R_L	symmet ry (see*)	K	K_v
1	1:4	17	0.09	40	0.0553	0.46	106	$1.17\cdot10^6$	a. s.	2.4	$7.83\cdot10^{-3}$
2	1:4	17	0.09	150	0.0393	0.7	106	$1.17\cdot10^6$	tr	1.12	$3.66\cdot10^{-3}$
3	1:4	17	0.09	250	0.0317	0.88	106	$1.17\cdot10^6$	s.	0.72	$2.35\cdot10^{-2}$
4	1:4	5	0.3	40	0.109	1.07	104	$3.45\cdot10^5$	a. s.	2.04	$1.22\cdot10^{-3}$
5	1:4	5	0.3	100	0.073	1.33	104	$3.45\cdot10^5$	s.	1.10	$6.62\cdot10^{-3}$
6	1:4	5	0.3	200	0.04	1.87	104	$3.45\cdot10^5$	s.	0.43	$2.58\cdot10^{-3}$
7	1:4	5	0.09	10	0.128	0.284	31	$3.45\cdot10^5$	s.	9.01	$5.42\cdot10^{-2}$
8	1:4	5	0.09	40	0.064	0.567	31	$3.45\cdot10^5$	s.	2.25	$1.35\cdot10^{-2}$
9	1:1	17	0.09	40	0.0553	0.46	106	$1.17\cdot10^6$	a. s.	2.40	$1.56\cdot10^{-2}$
10	1:1	17	0.09	150	0.0393	0.76	106	$1.17\cdot10^6$	s.	1.12	$7.31\cdot10^{-3}$
11	1:1	17	0.09	250	0.0317	0.88	106	$1.17\cdot10^6$	s.	0.72	$4.70\cdot10^{-3}$

* s. -symmetric regim , a. s. - antisymmetric regim , tr - transient regim (between symmetric and antisymmetric)

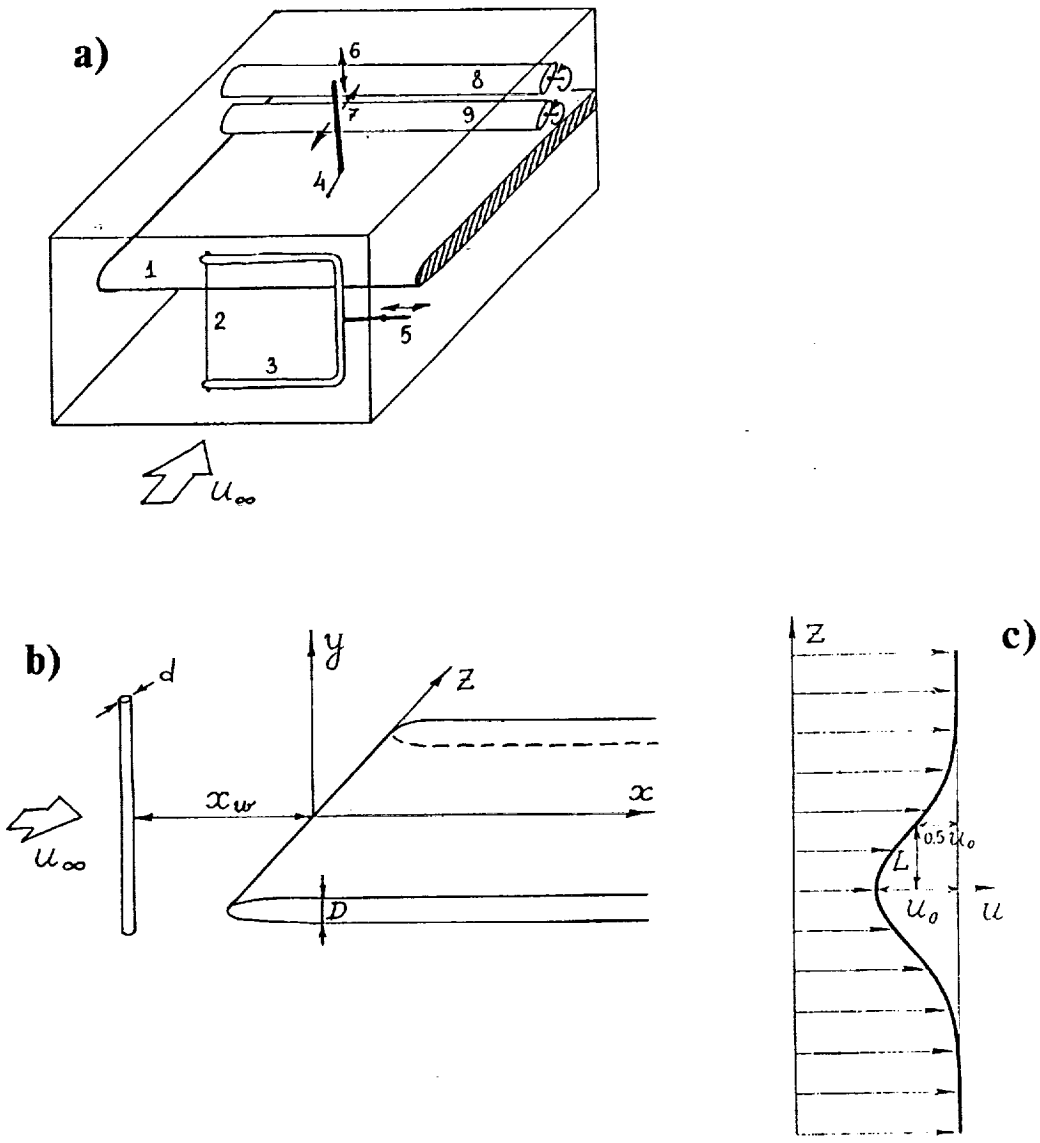

Figure 1. (a) - Experimental setup; 1 - plate, 2 - wire, 3 - wire holder, 4 - probe, 5 - wire holder movment, 6, 7 - probe movements, 8, 9 - flaps.
(b) - coordinate system and general designations
(c) - wake parameters: u_o - velocity deficite, L - half-width.

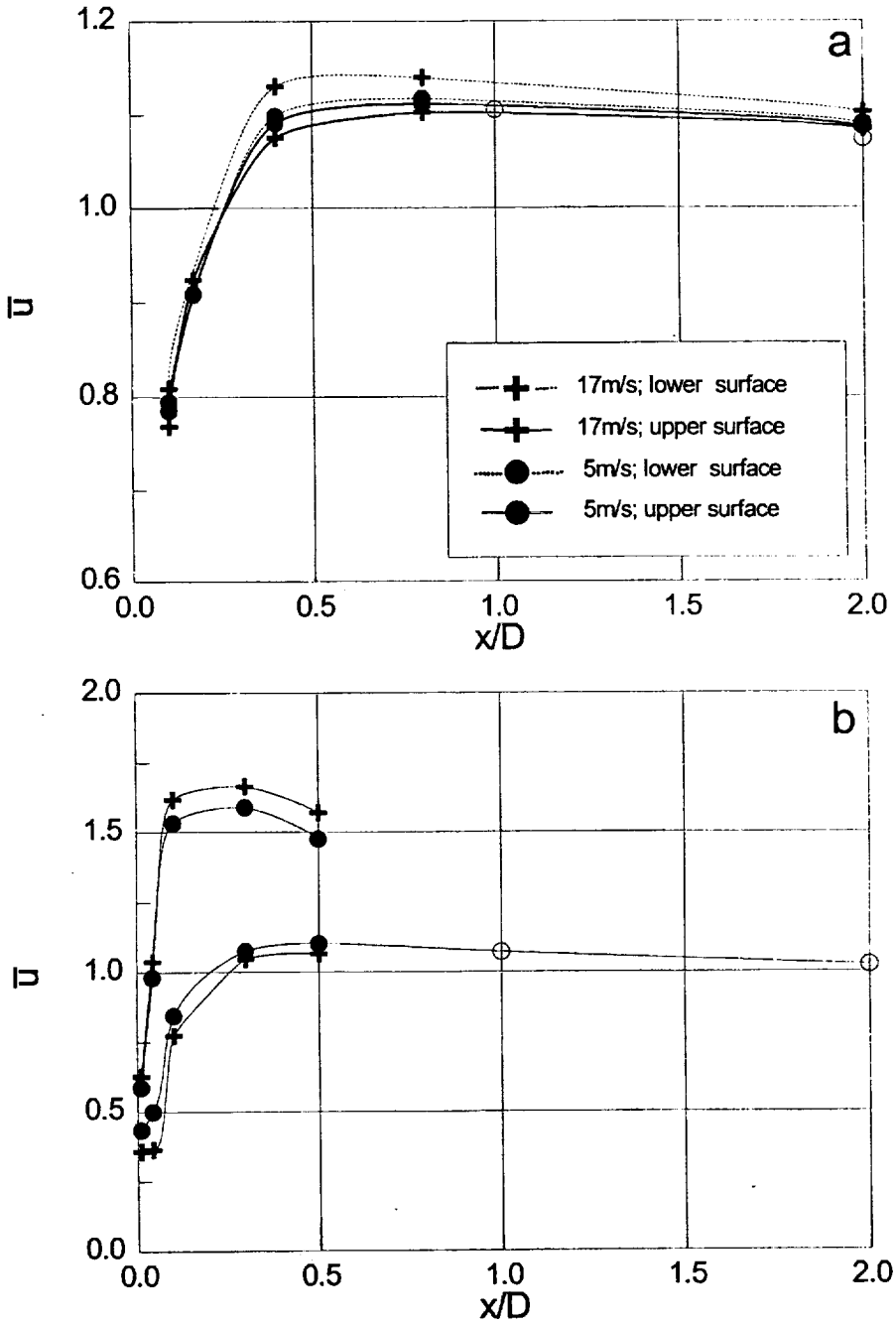

Figure 2. Velocity distributions over nose
a - nose 1:4
b - nose 1:1

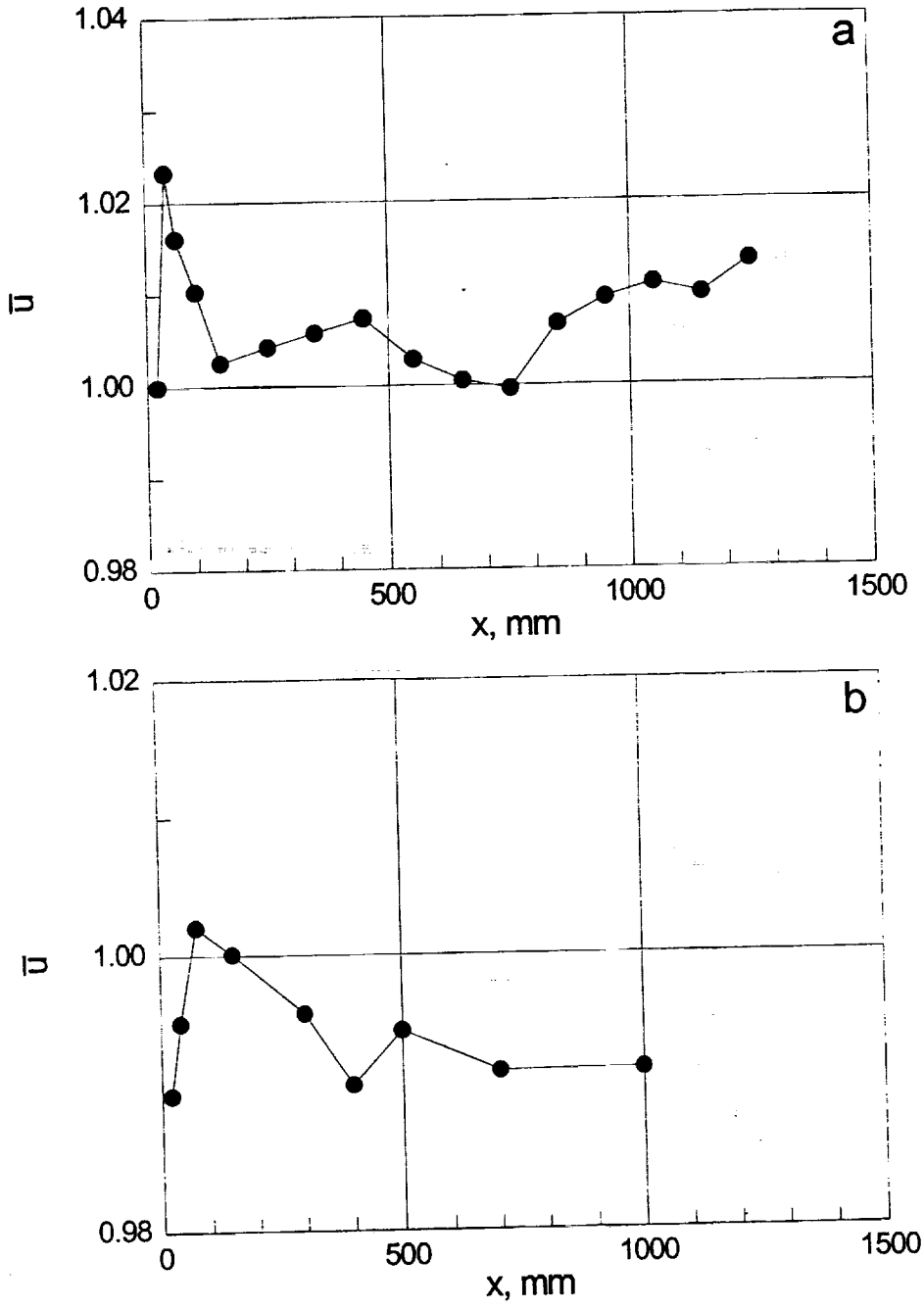

Figure 3. Velocity distributions over plate surface for U_∞=5m/s measured at y=40mm
a - nose 1:4
b - nose 1:1

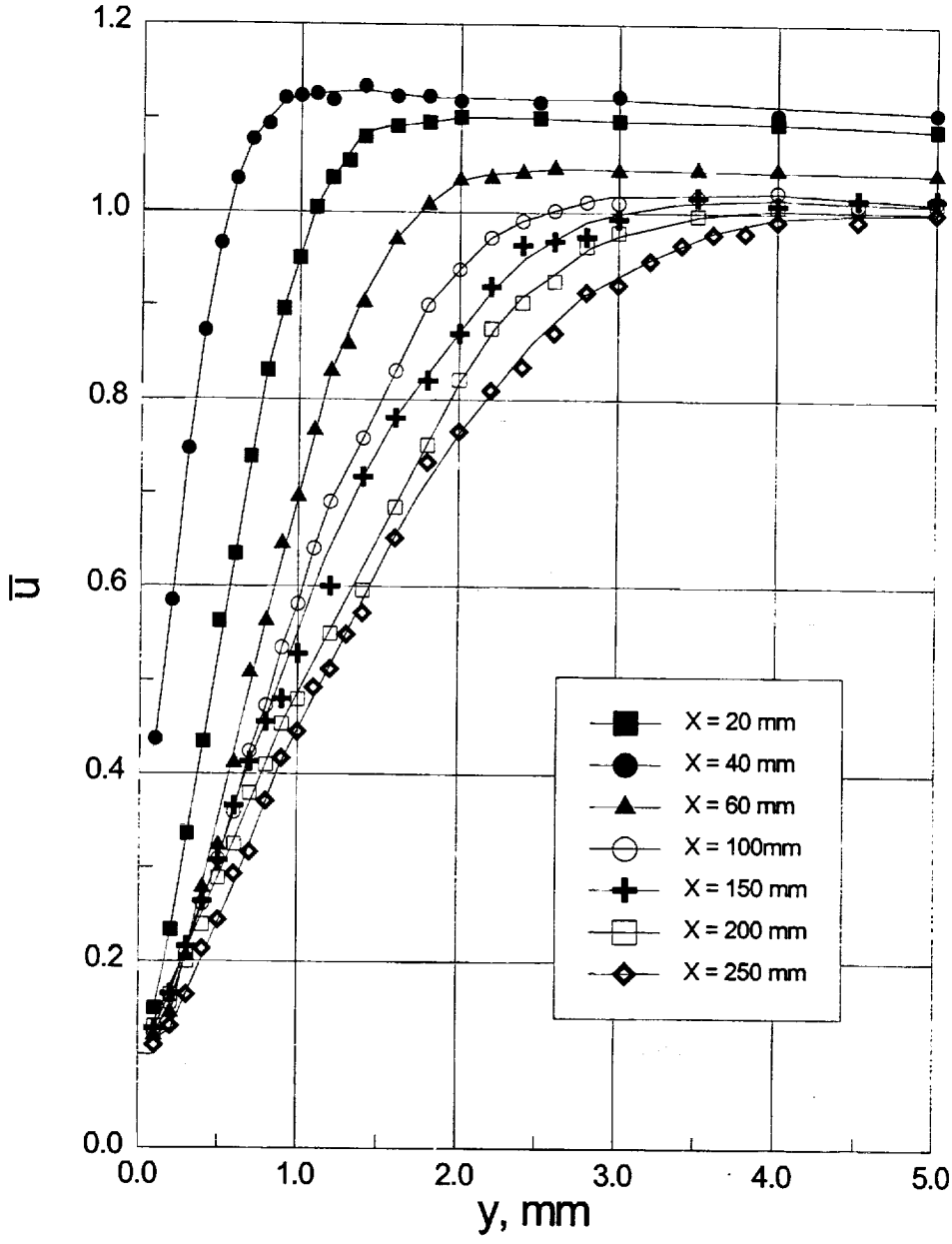

Figure 4. Velocity profiles in boundary layer over plate with nose 1:4; U_∞=5m/s.

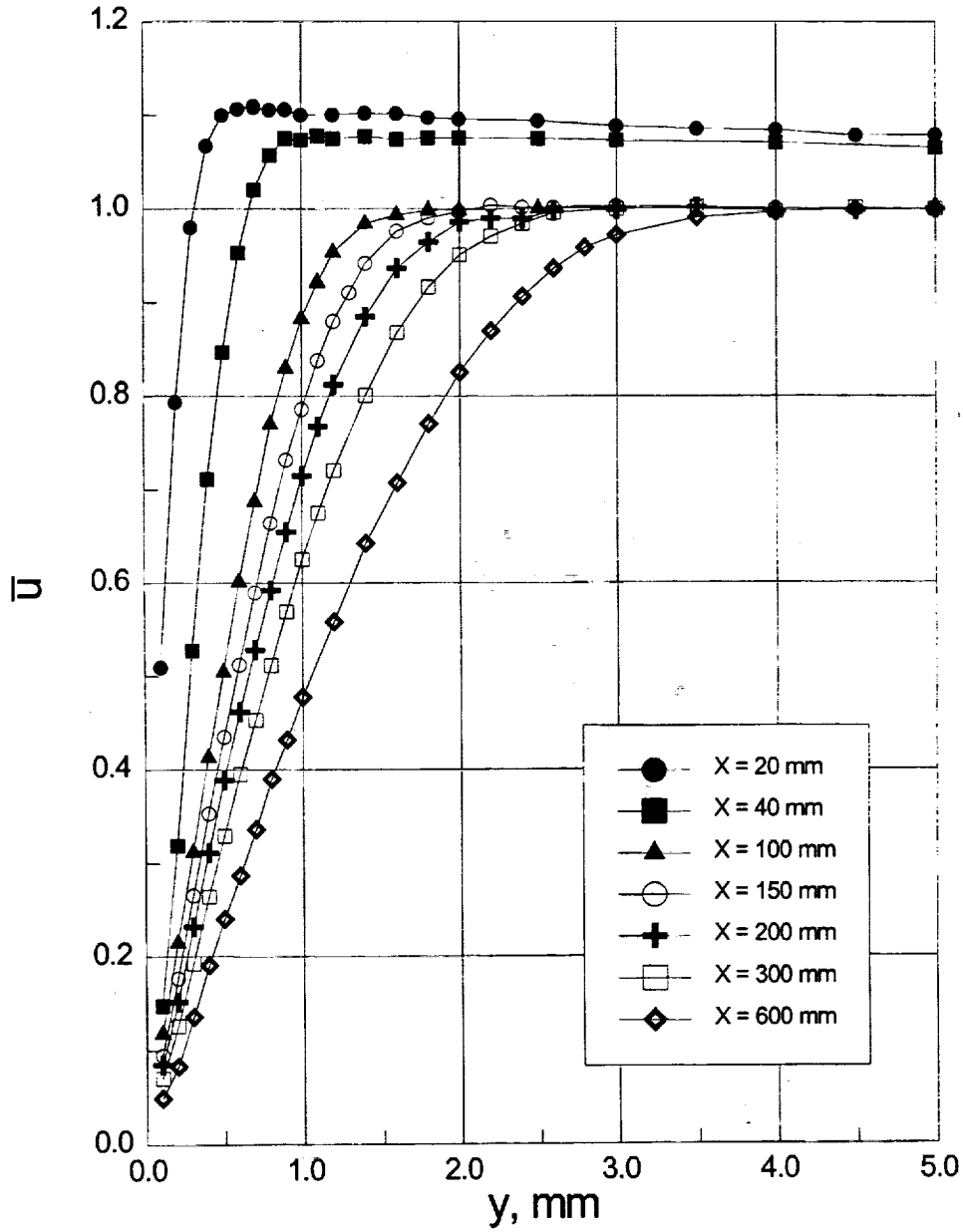

Figure 5. Velocity profiles in boundary layer over plate with nose 1:4; U_{∞}=17m/s.

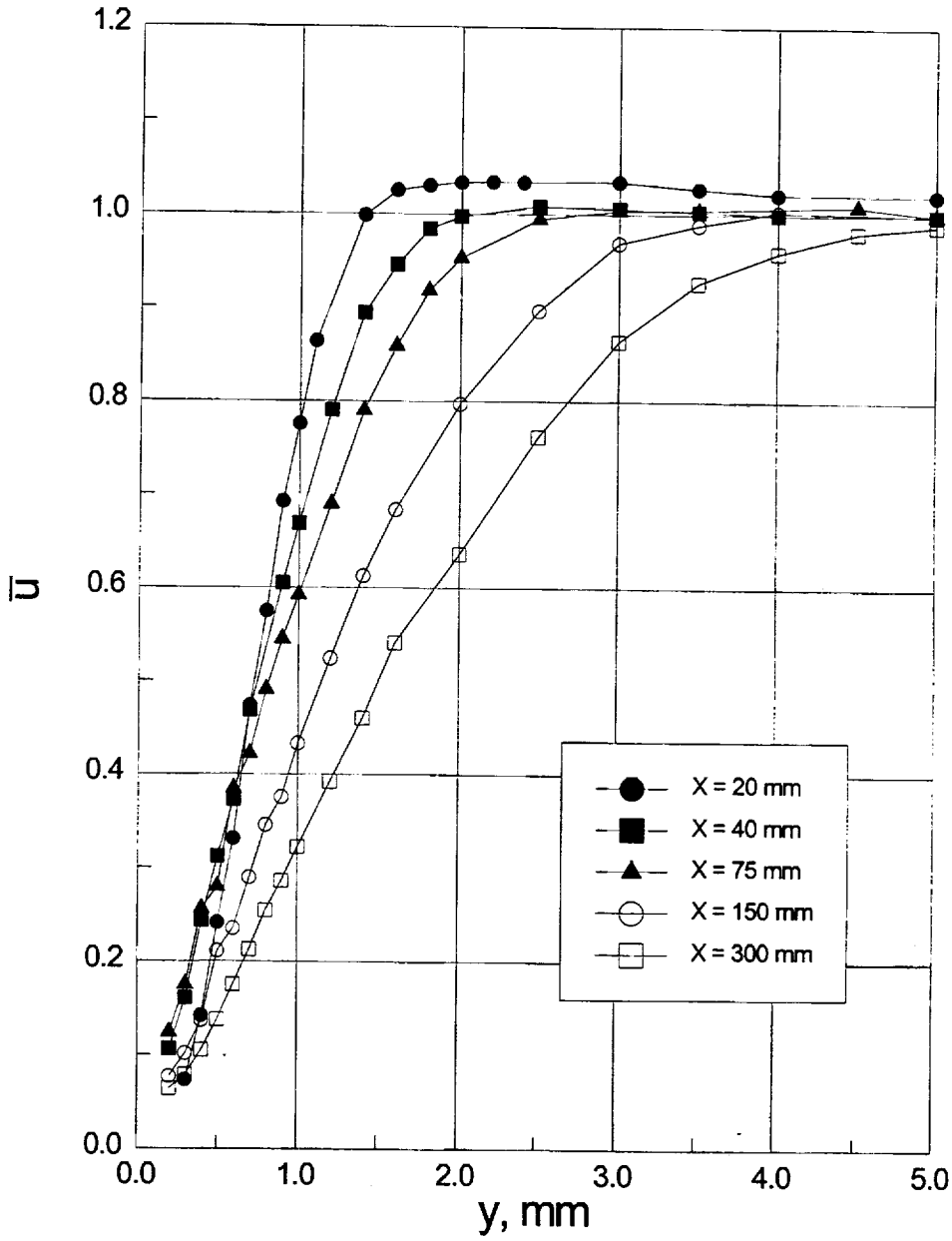

Figure 6. Velocity profiles in boundary layer over plate with nose 1:1; U_∞=5m/s.

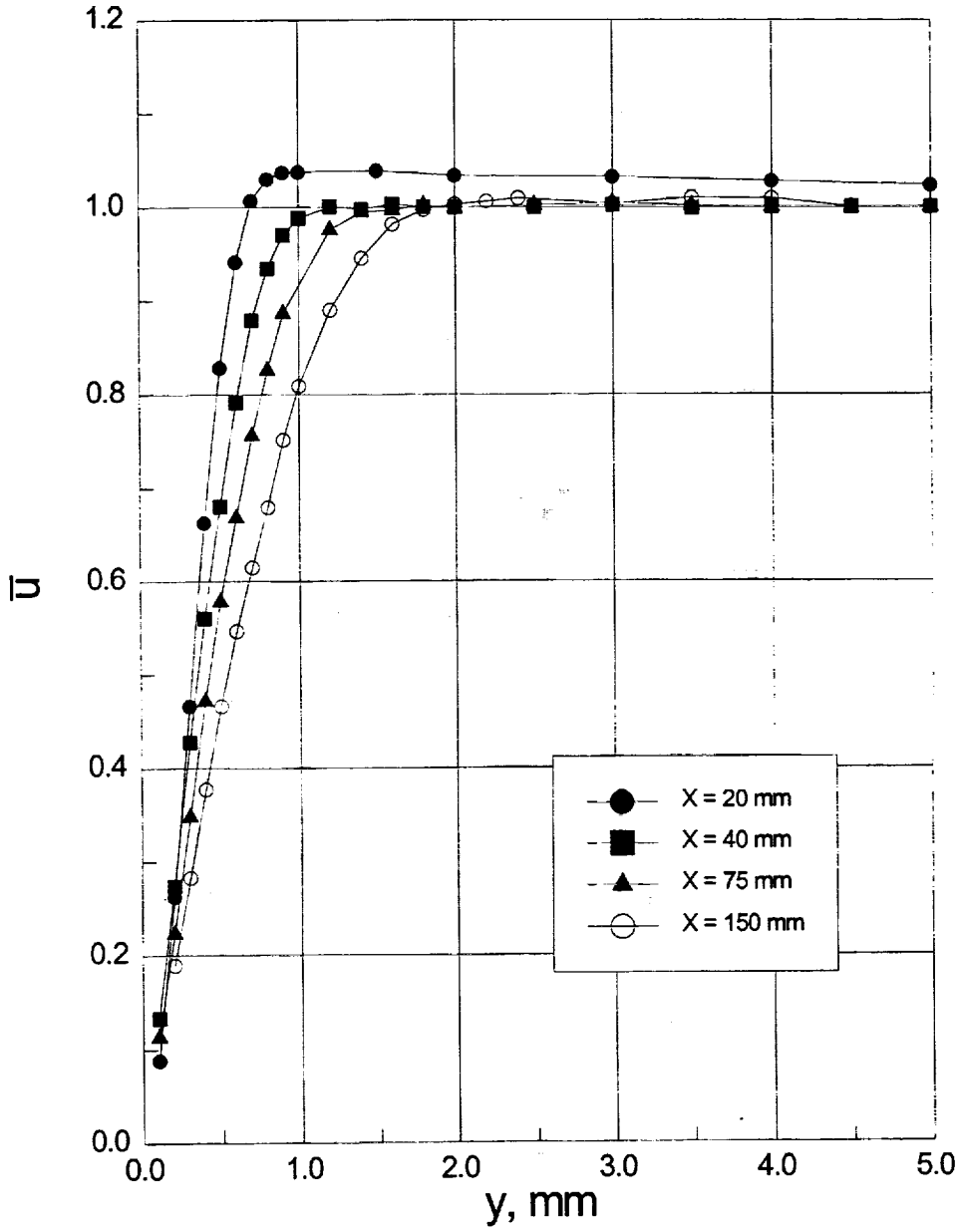

Figure 7. Velocity profiles in boundary layer over plate with nose 1:1; U_∞=17m/s.

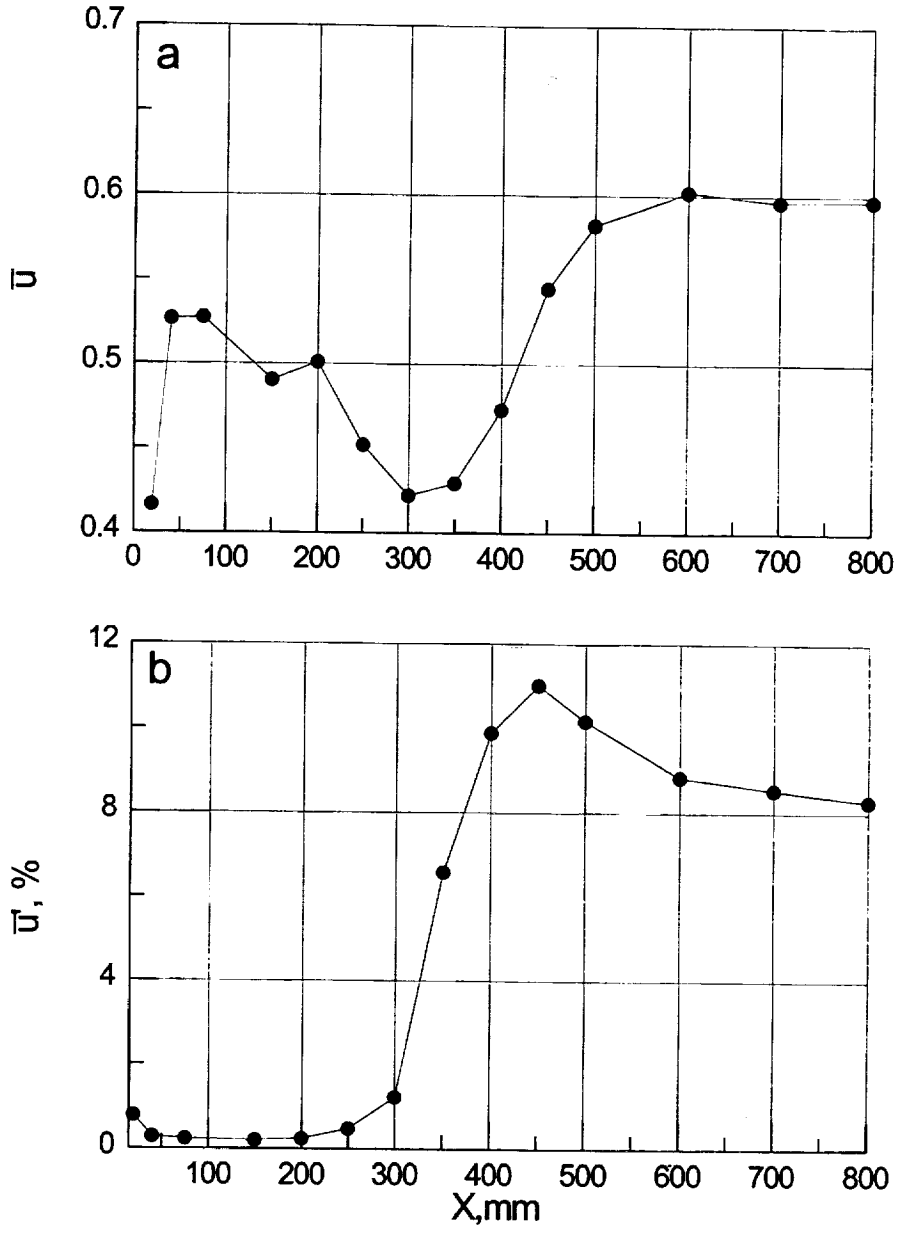

Figure 8. Mean flow velocity (a) and pulsations (b) in boundary layer over plate with nose 1:1 at U_{∞}=17m/s.

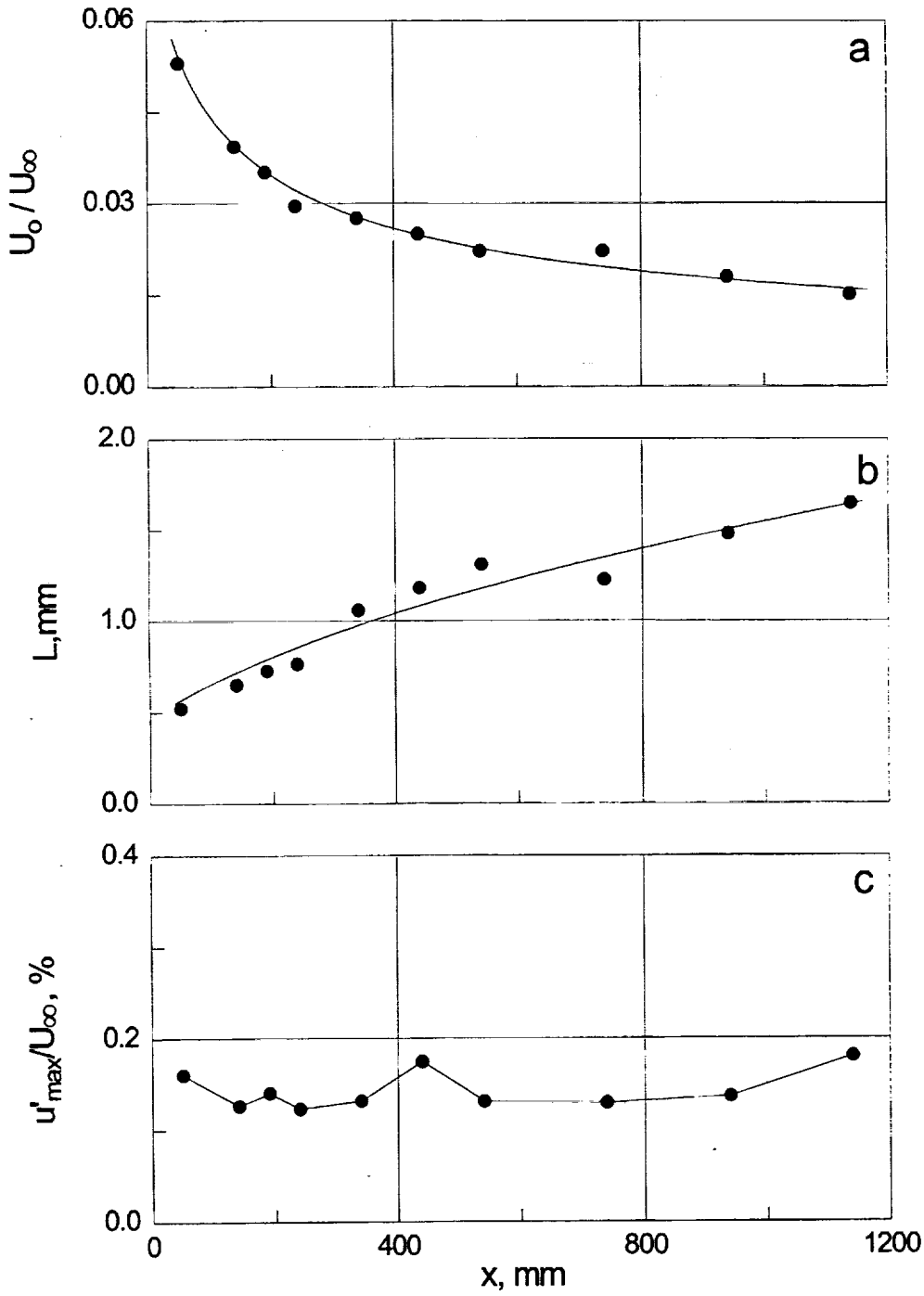

Figure 9. Wake behind wire of d=0.09mm in flow with U_∞=17m/s
a) velocity deficite U_o / U_∞;
b) half width L;
c) pulsations u'_{max}/U_∞.

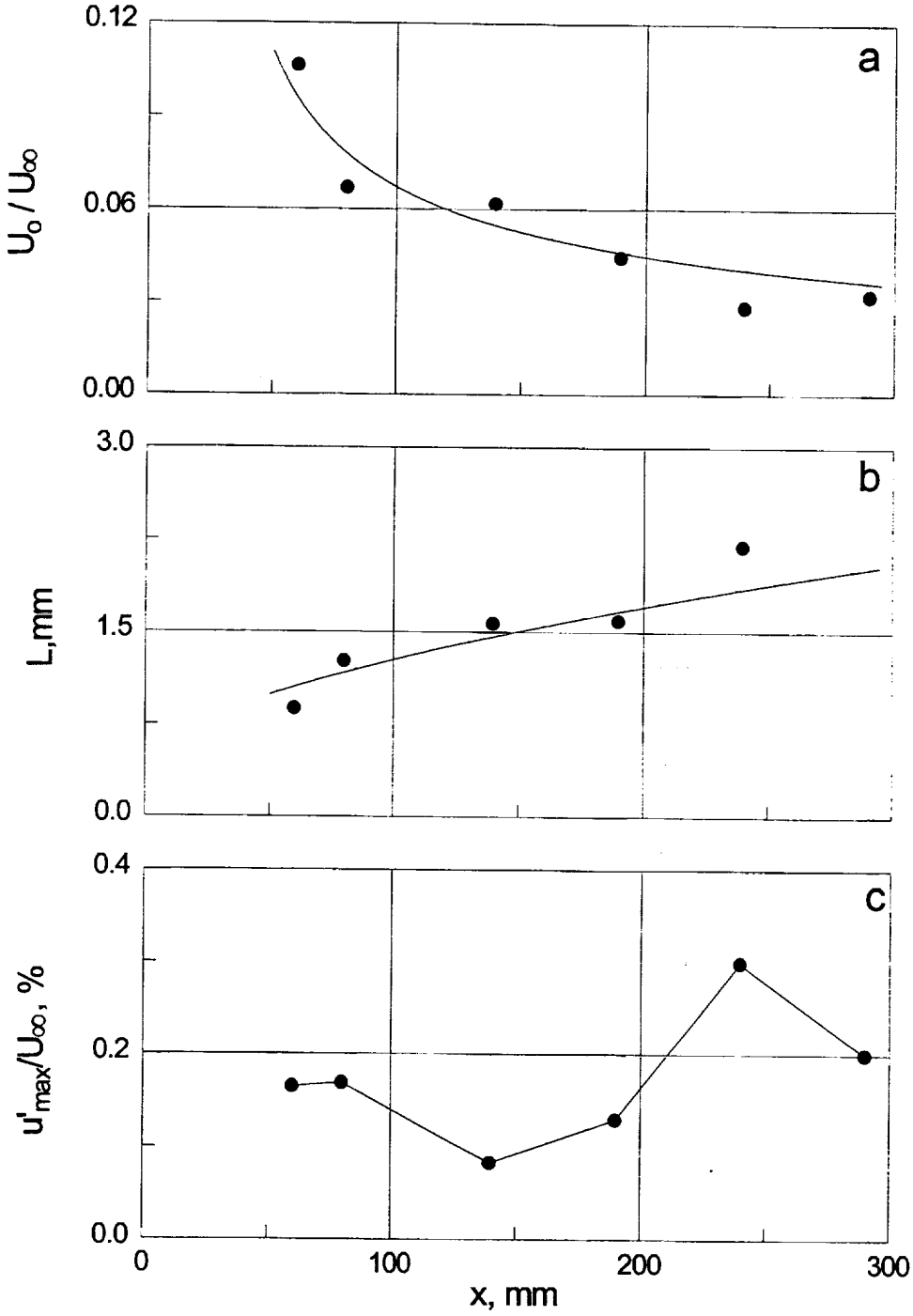

Figure 10. Wake behind wire of d=0.3mm in flow with U_∞=5m/s
a) velocity deficite U_o / U_∞;
b) half width L
c) pulsations u'_{max}/U_∞.

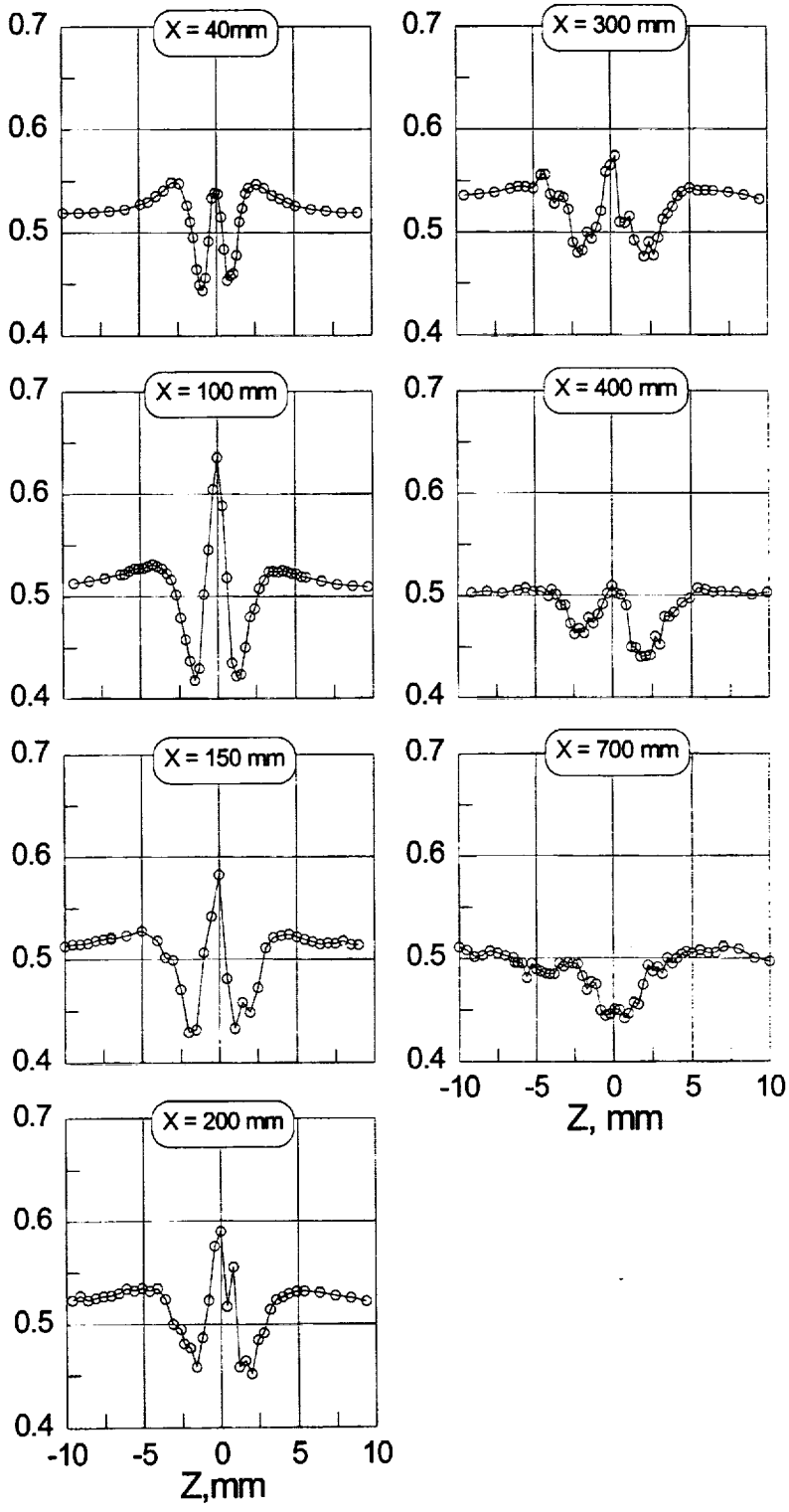

Figure 11. Flow distortion in boundary layer in configuration 3.
U_∞ =17 m/s; nose 1:4; d = 0.09 mm; x_w = 250 mm

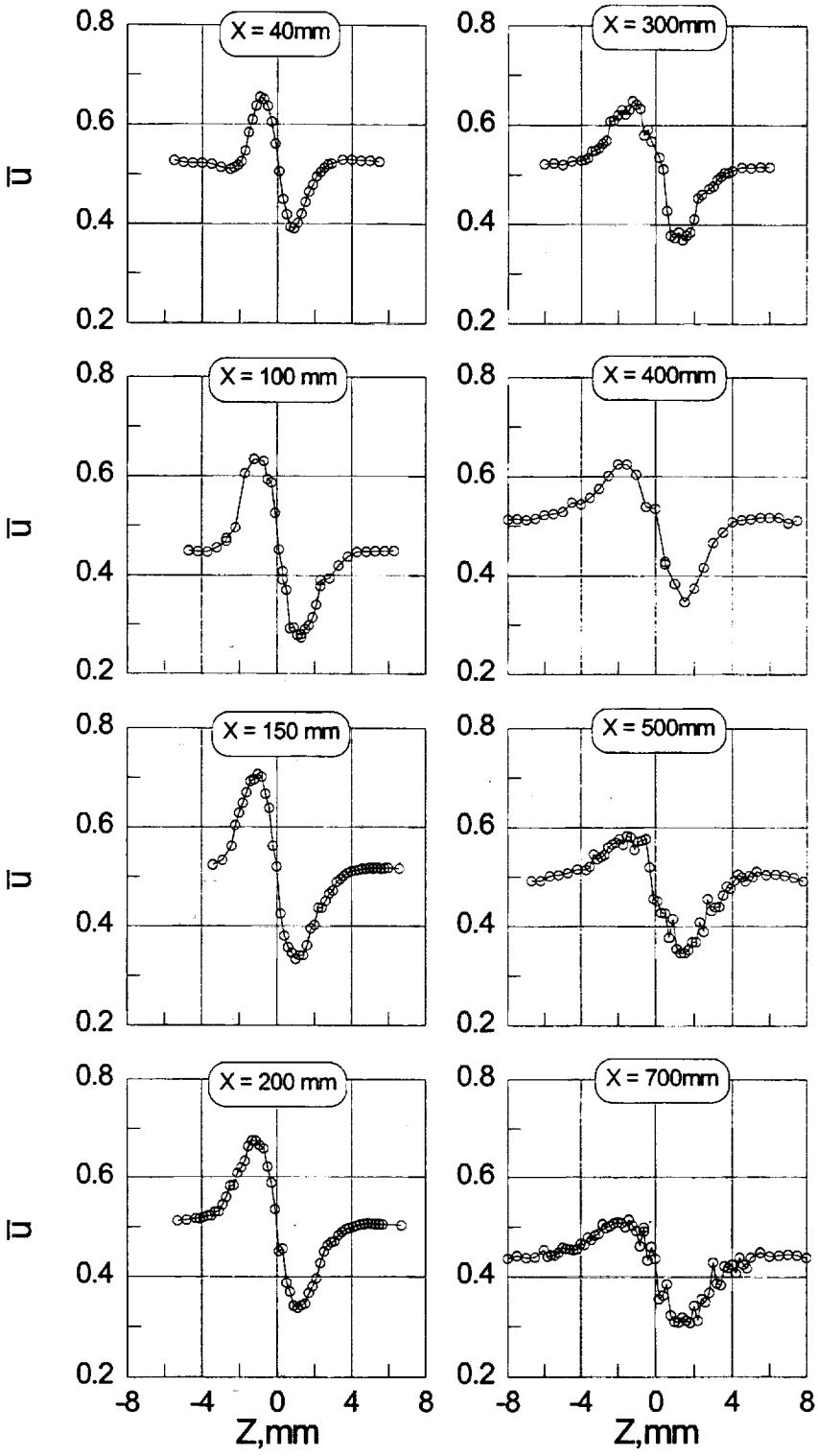

Figure 12. Flow distortion in boundary layer in configuration 1.
U_∞ =17 m/s; nose 1:4; d = 0.09 mm; x_w = 40 mm

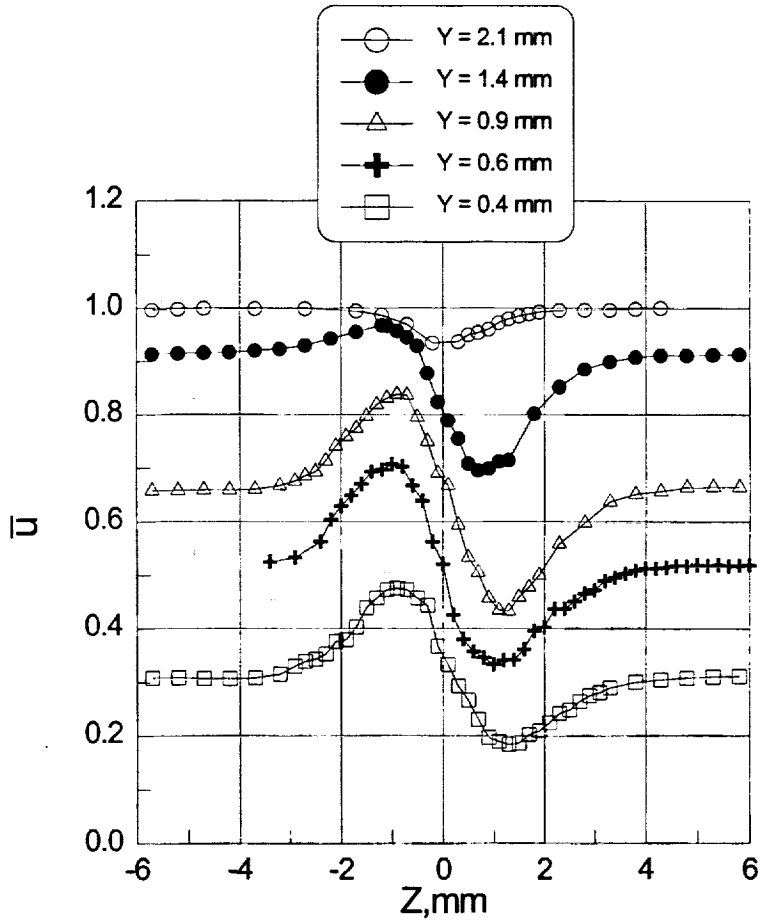

Figure 13. Velocity distribution in (y,z) plane at x = 150 mm
for flow configuration 1
U_∞ = 17 m/s; nose 1:4; d = 0.09 mm; x_w = 40 mm.

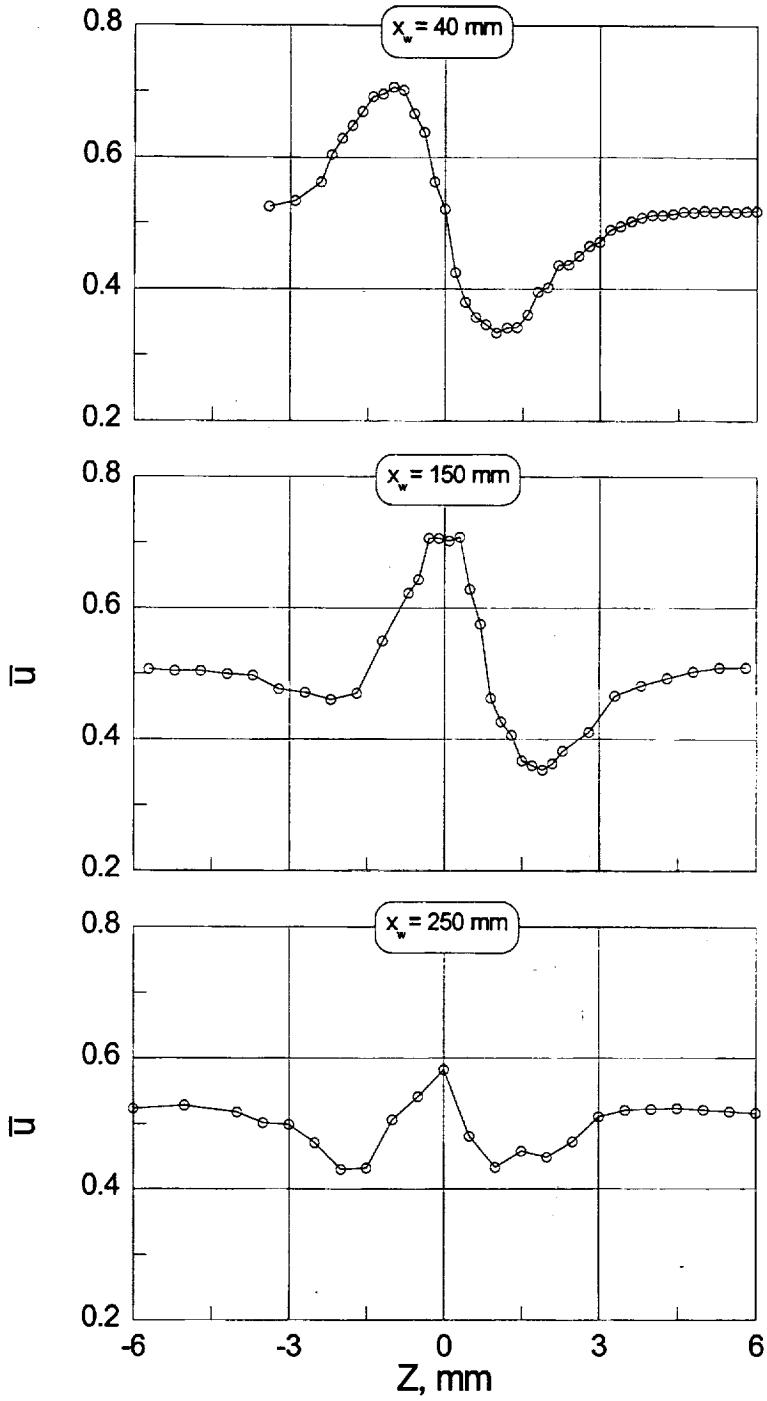

Figure 14. Velocity distribution at x = 150 mm
U_∞ = 17 m/s; nose 1:4; d = 0.09 mm

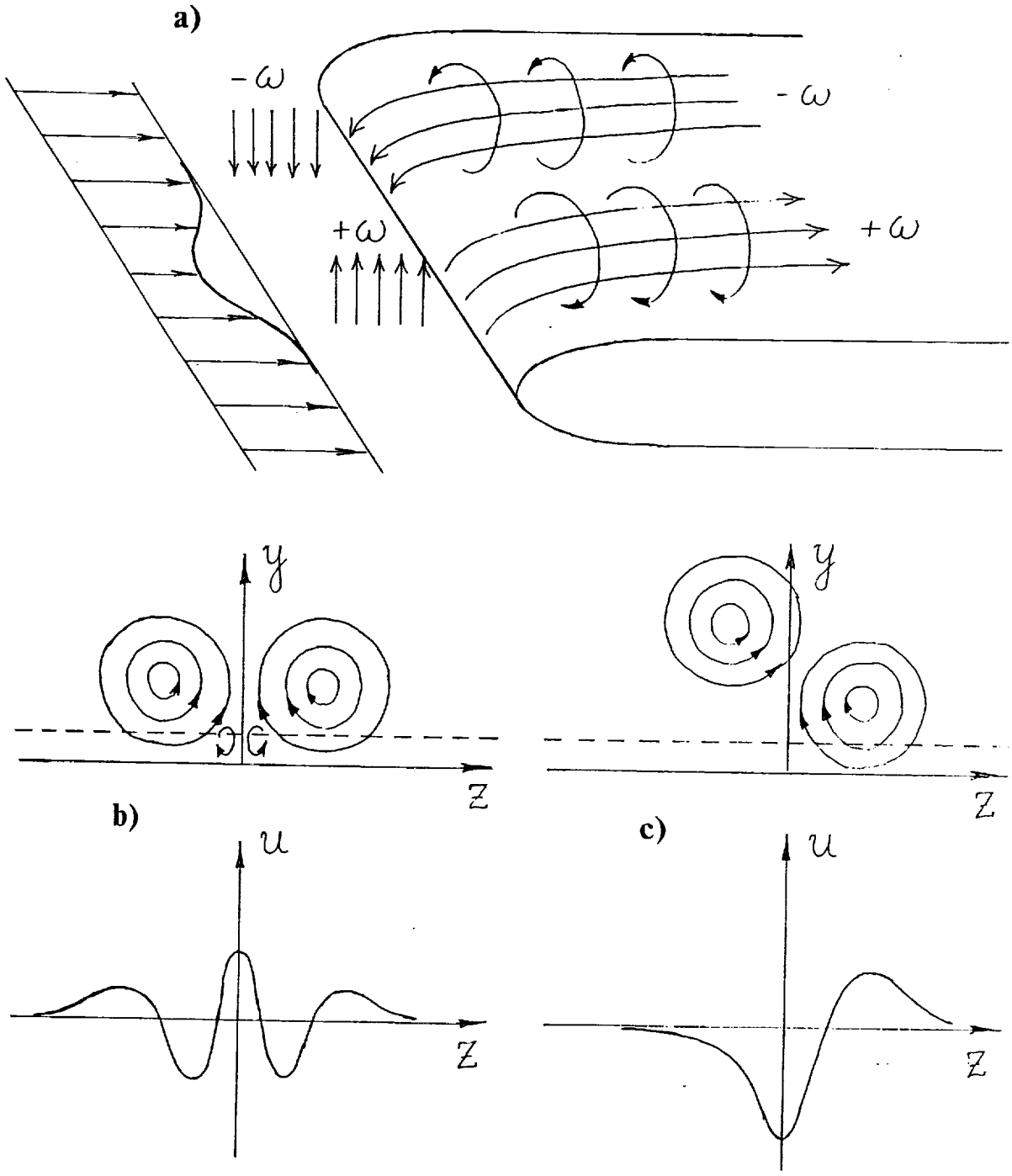

Figure 15 (a) - Vorticity lines deformation over leading edge
(b) - Flow in *(y,z)* plane and spanwise distribution of velocity in boundary layer for symmetric regime.
(c) - the same for antisymmetric regime.

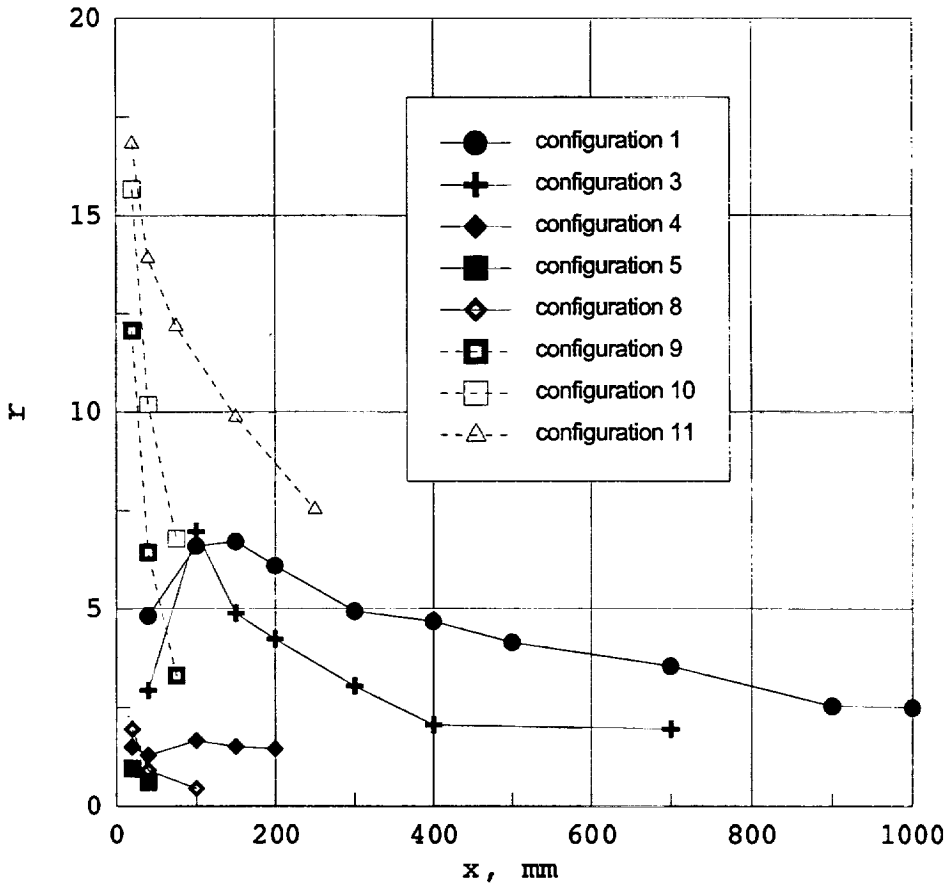

Figure 16. Amplification coefficient $r = \Delta U_b/U_{ole}$
for various flow configurations.

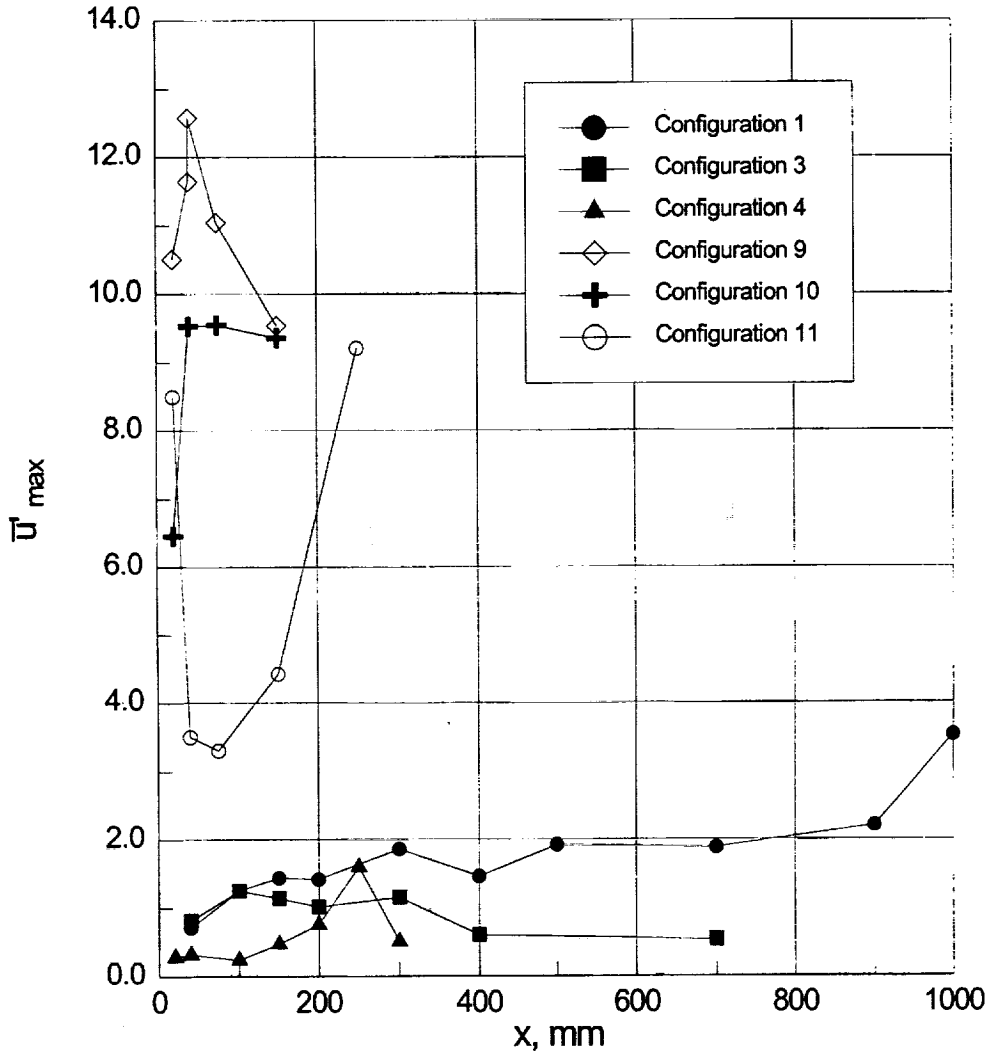

Figure 17. Maximun pulsations $\overline{u}'_{max}$ in boundary layer for various flow configurations.

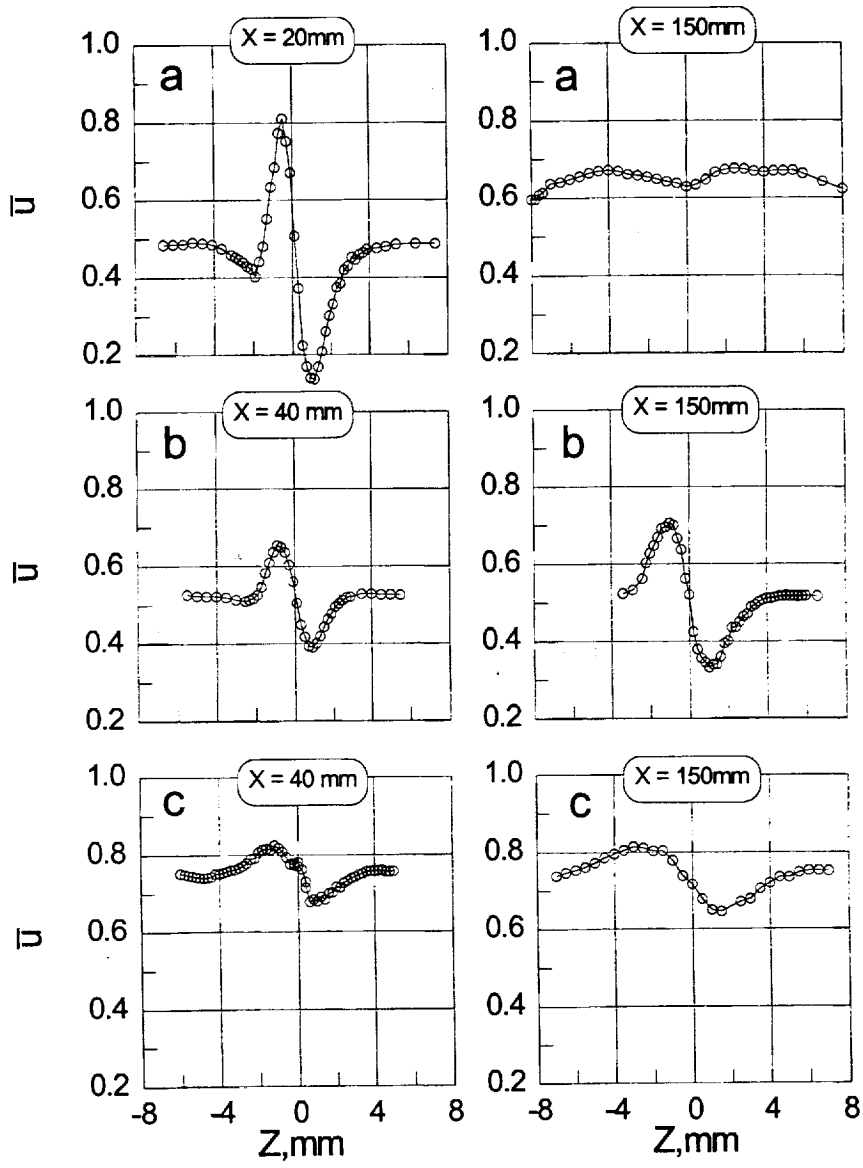

Figure 18. Flow distortion in boundary layer.
a)configuration 9; U_∞ =17 m/s; d = 0.09 mm; x_w = 40 mm; nose 1:1
b)configuration 1; U_∞ =17 m/s; d = 0.09 mm; x_w = 40 mm; nose 1:4
c)configuration 4; U_∞ = 5 m/s; d = 0.3 mm; x_w = 40 mm; nose 1:4

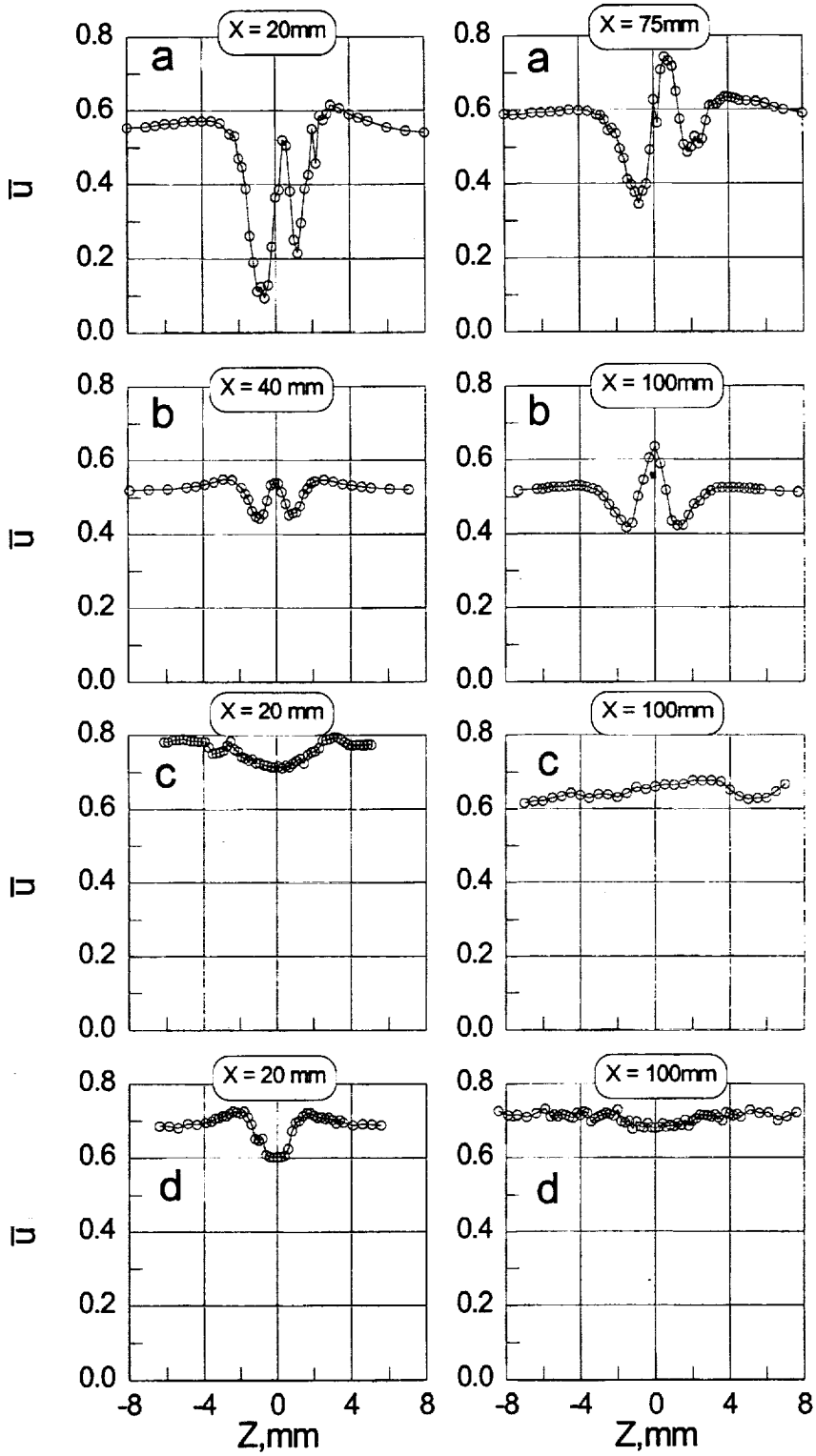

Figure 19. Flow distortion in boundary layer.
a)configuration 11; U_∞ =17 m/s; d = 0.09 mm; x_w = 250 mm; nose 1:1
b)configuration 3; U_∞ =17 m/s; d = 0.09 mm; x_w = 250 mm; nose 1:4
c)configuration 5; U_∞ = 5 m/s; d = 0.3 mm; x_w = 100 mm; nose 1:4
d)configuration 8; U_∞ = 5 m/s; d = 0.3 mm; x_w = 40 mm; nose 1:4

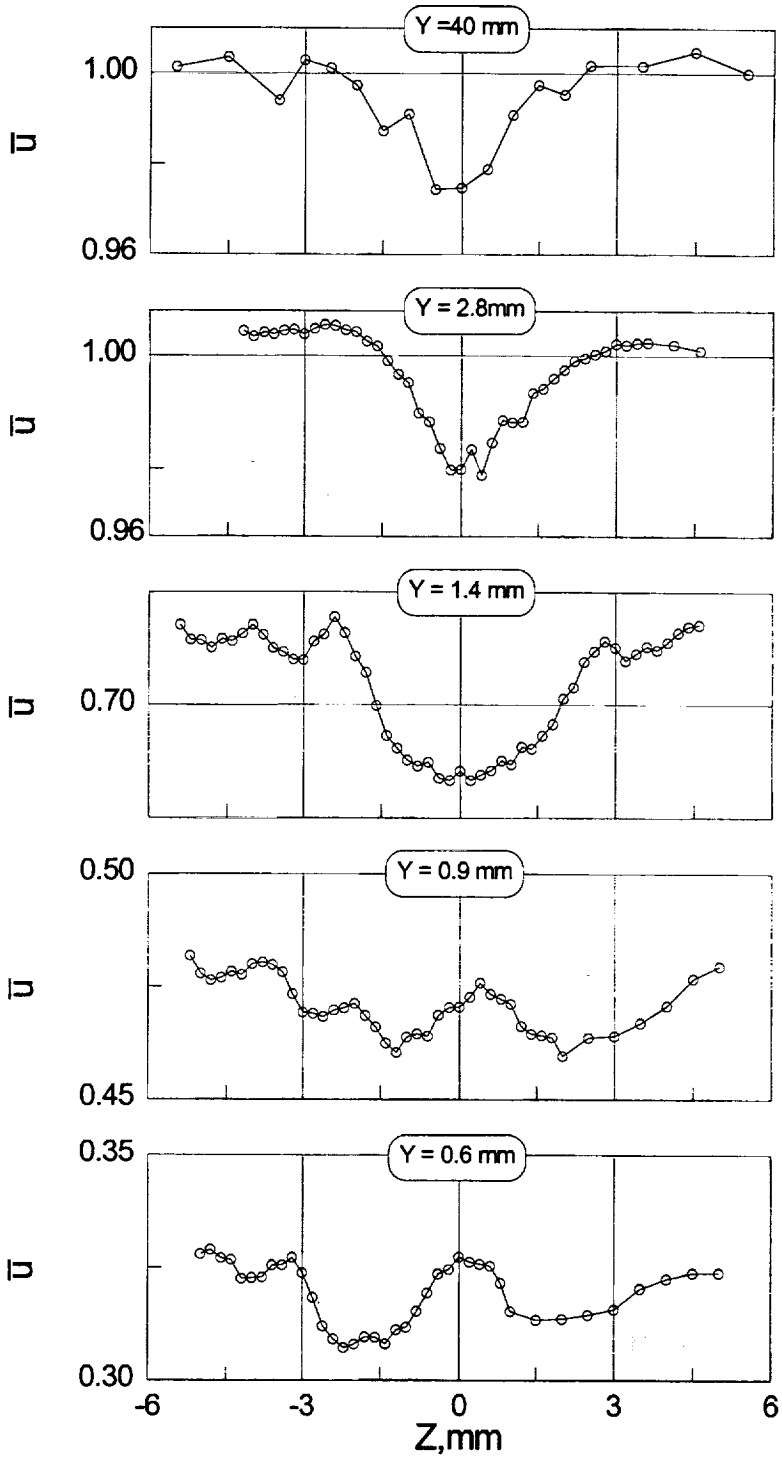

Figure 20. Velocity distribution in (y,z) plane at x = 100 mm
for flow configuration 5
U_∞ = 5 m/s; nose 1:4; d = 0.09 mm; x_w = 40 mm;

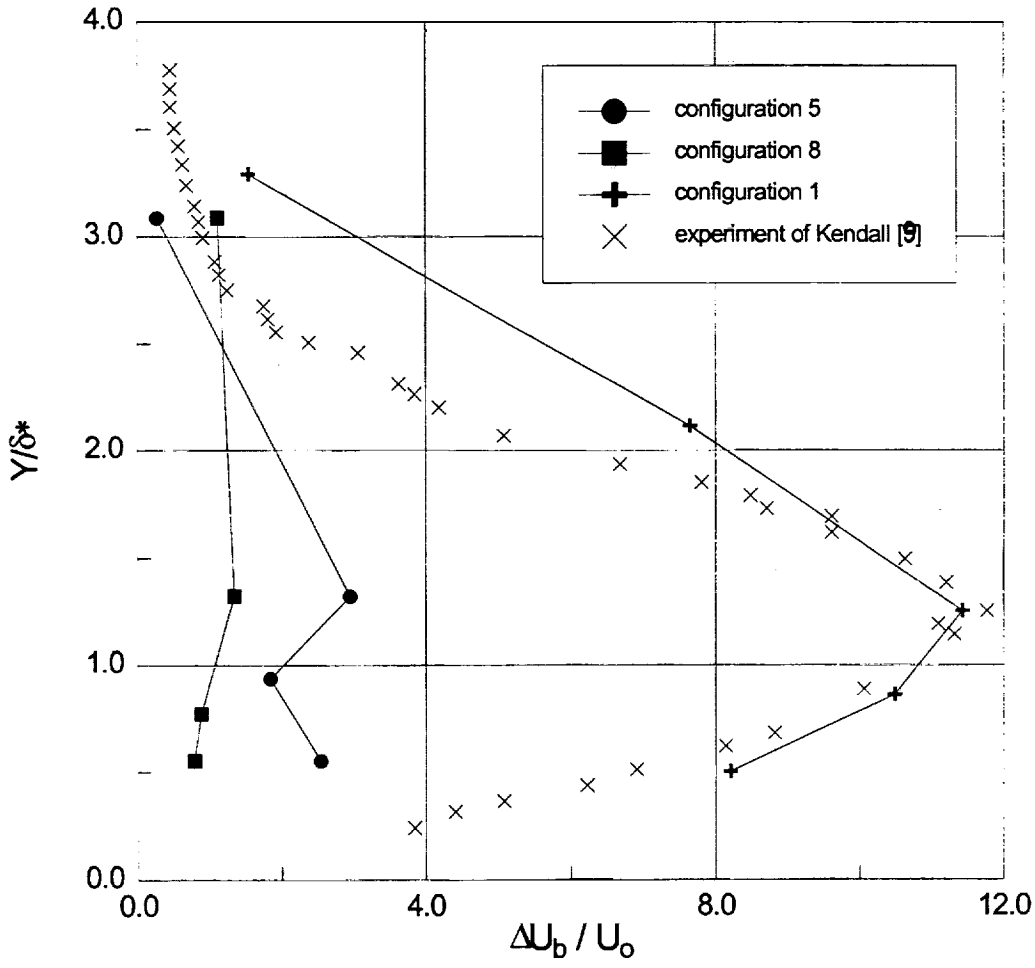

Figure 21. Profiles of maximal flow distortion in boundary layer.

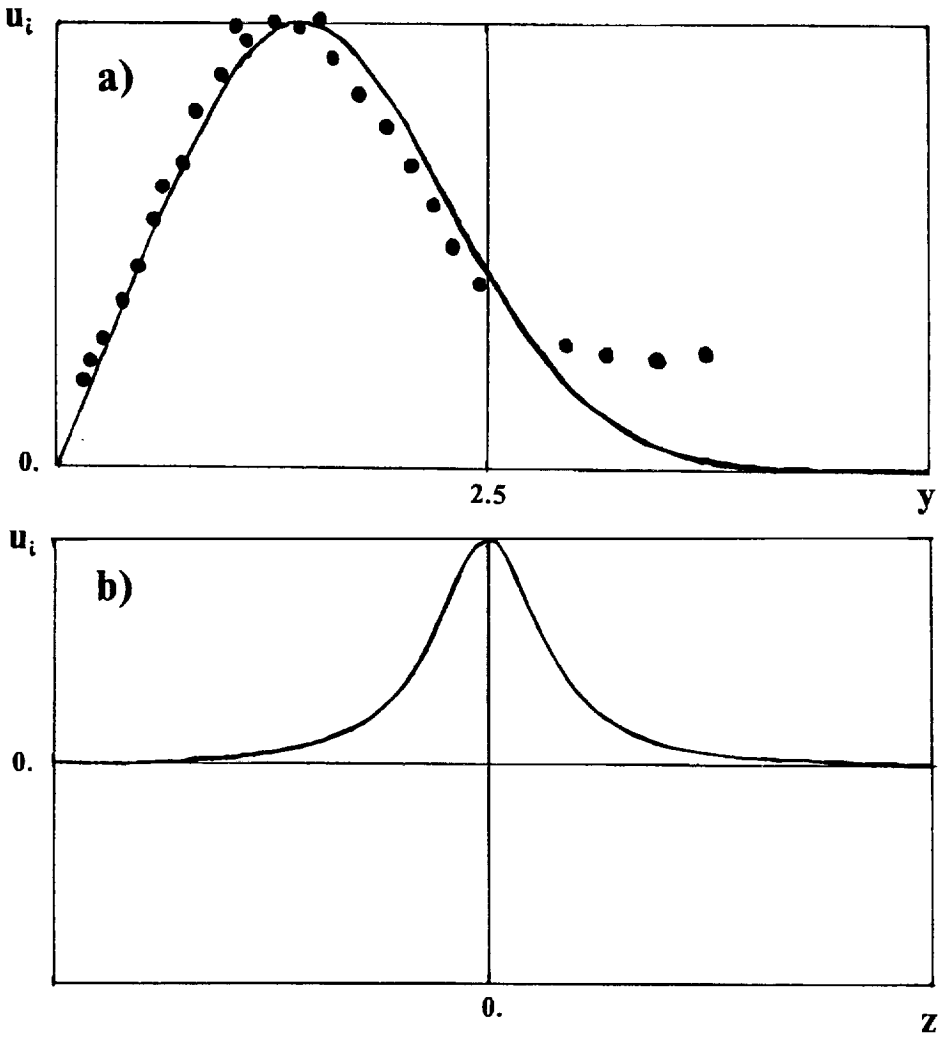

Figure 22. Vertical (a) and spanwise (b) profiles of flow inhomogeneity

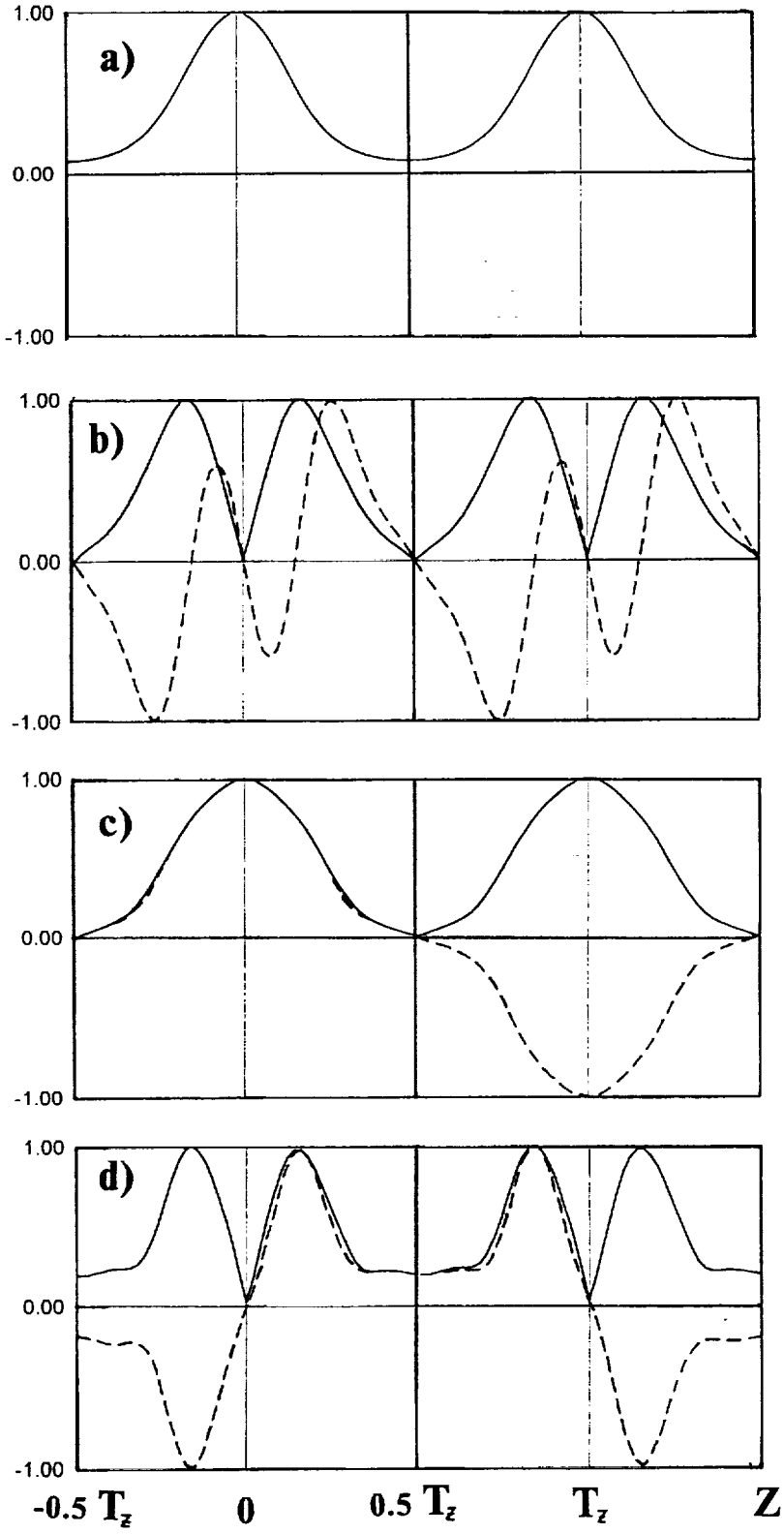

Figure 23. **Spanwise distributions of streamwise velocity of disturbances *Re(U)* (-----) and it's amplitude $|U|$ (———) in harmonically modulated flow with *a=-0.3, =0.25, =0.6***
(a), (b) - symmetric and antisymmetric fundamental modes
(c), (d) - symmetric and antisymmetric subharmonic modes

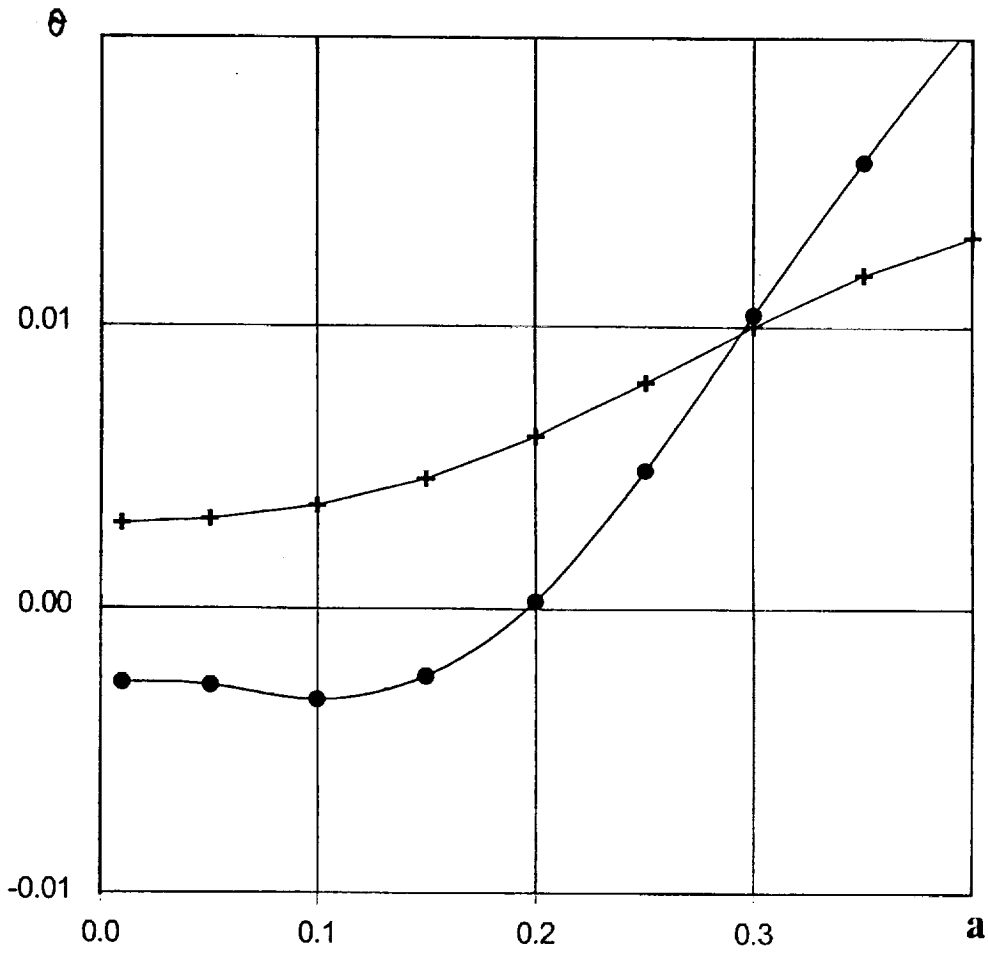

Figure 24. Growth rates of symmetric (— + —) and antisymmetric (—●—) modes as functions of modulation amplitude a in flow with $\alpha = 0.25$, $\beta = 0.6$.

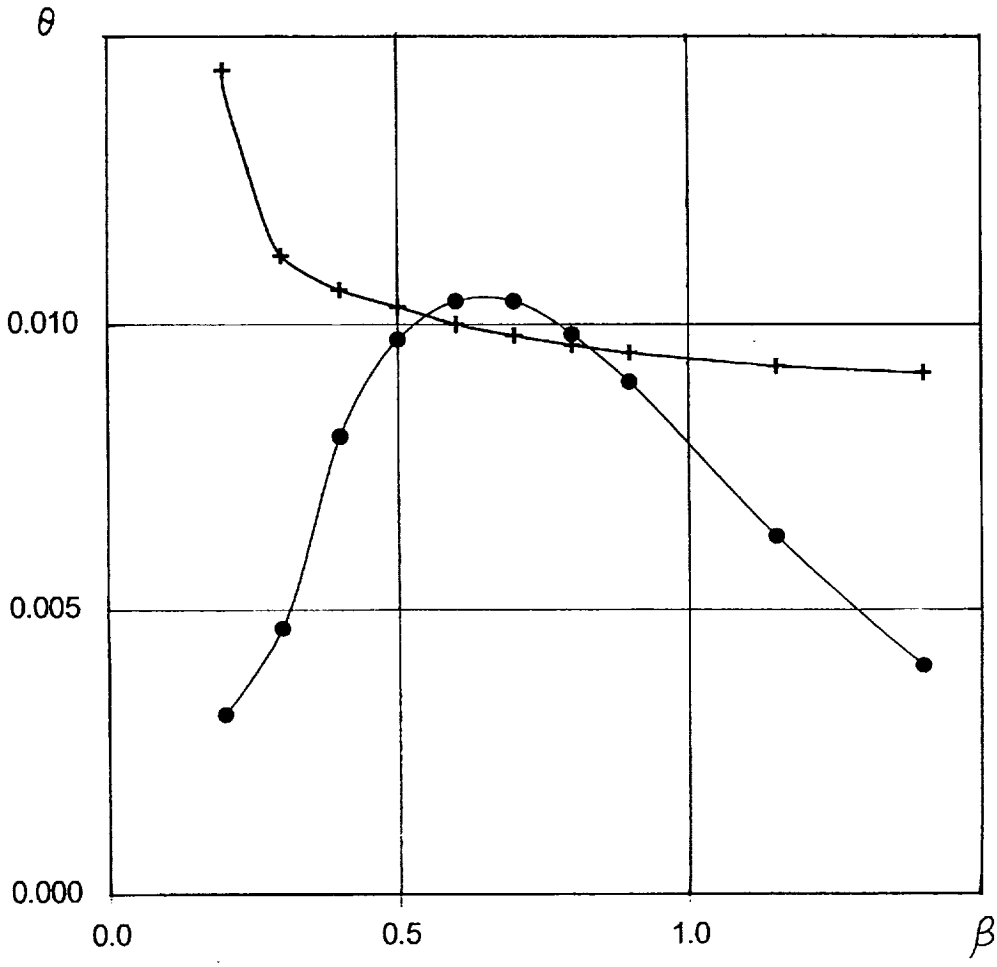

Figure 25. Growth rates of symmetric (– + —) and antisymmetric (—•—) modes as functions of β in flow with $\alpha = 0.25$, $a = -0.3$.

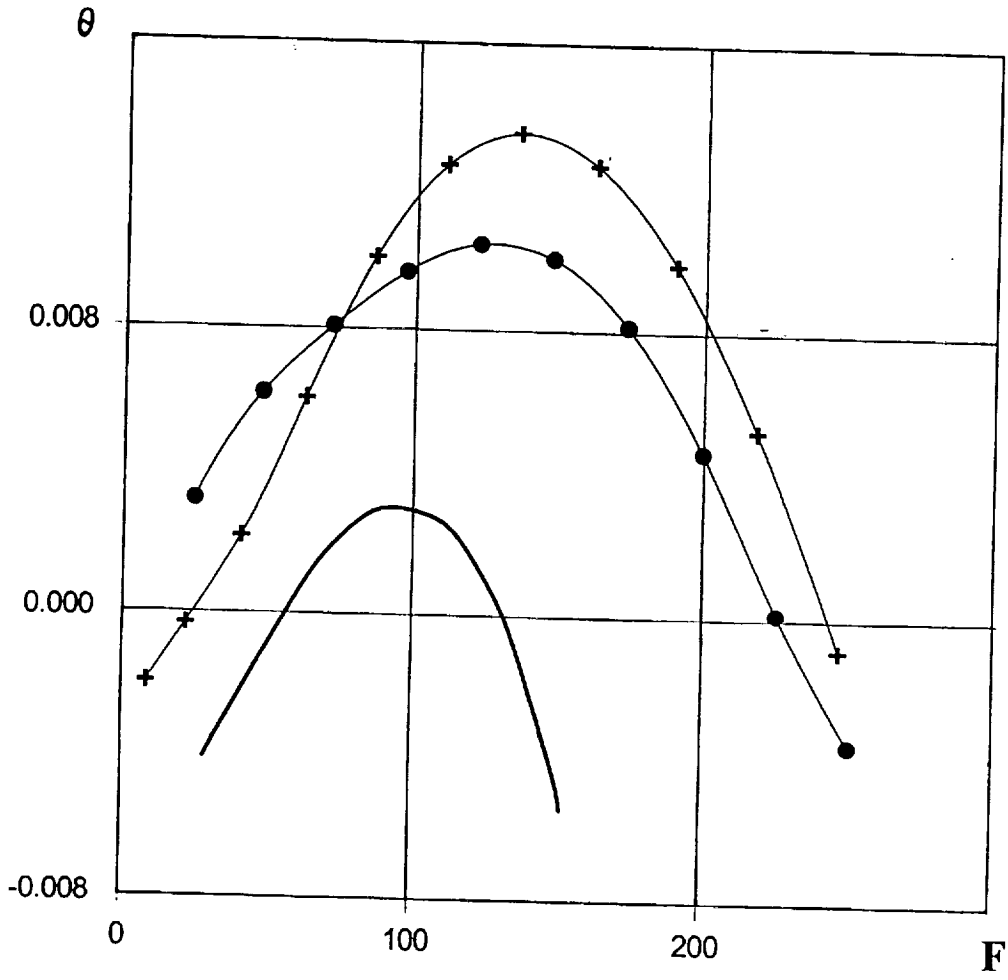

Figure 26. Growth rates v.s. reduced frequency *F*. Symmetric (—+—) and antisymmetric (—●—) modes for a=-0.3, β=0.6; (———) -TS waves

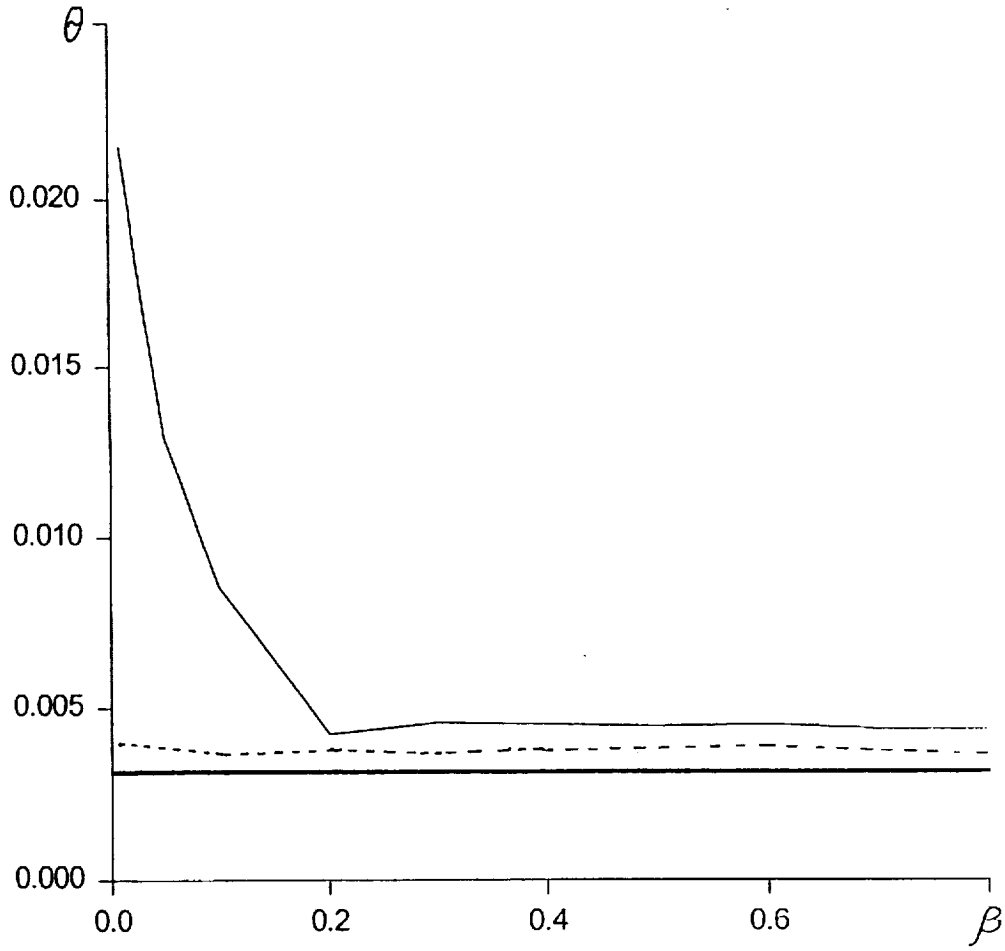

Figure 27. Growth rates v.s β for localized inhomogeneity flow (3.6) with $q=0.6$; (———) - $a=-0.3$; (- - - -) - $a=+0.3$; (▬▬▬) - TS wave

REPORT DOCUMENTATION PAGE

Form Approved
OMB No. 0704-0188

1. AGENCY USE ONLY (*Leave blank*)	2. REPORT DATE	3. REPORT TYPE AND DATES COVERED
	December 1997	Contractor Report

4. TITLE AND SUBTITLE
Receptivity of Flat-Plate Boundary Layer in a Non-Uniform Free Stream (Vorticity Normal to the Plate)

5. FUNDING NUMBERS
NCC1-241

282-10-01-01

6. AUTHOR(S)
M. N. Kogan and M. V. Ustinov

7. PERFORMING ORGANIZATION NAME(S) AND ADDRESS(ES)
Central Aerohydrodynamics Institute (TsAGI)
Zhukovski
Moscow Region
140160
Russia

8. PERFORMING ORGANIZATION REPORT NUMBER

9. SPONSORING / MONITORING AGENCY NAME(S) AND ADDRESS(ES)
National Aeronautics and Space Administration
Langley Research Center
Hampton, VA 23681-2199

10. SPONSORING / MONITORING AGENCY REPORT NUMBER
NASA/CR-97-206273

11. SUPPLEMENTARY NOTES
Langley Technical Monitor: Dennis M. Bushnell

12a. DISTRIBUTION / AVAILABILITY STATEMENT
Unclassified - Unlimited
Subject Category 34
Distribution: Standard
Availability: NASA CASI (301) 621-0390

12b. DISTRIBUTION CODE

13. ABSTRACT (*Maximum 200 words*)

Work is devoted to study of free-stream vorticity normal to leading edge interaction with boundary layer over plate and resulting flow distortion influence on laminar-turbulent transition. In experiments made the wake behind the vertically stretched wire was used as a source of vortical disturbances and its effect on the boundary layer over the horizontally mounted plate with various leading edge shapes was investigated. The purpose of experiments was to check the predictions of theoretical works of M.E. Goldstein, et. al. This theory shows that small free-stream inhomogeneity interacting with leading edge produces considerable distortion of boundary layer flow. In general, results obtained confirms predictions of Goldstein's theory, i.e., the amplification of steady vortical disturbances in boundary layer caused by vortex lines stretching was observed. Experimental results fully coincide with predictions of theory for large Reynolds number, relatively sharp leading edge and small disturbances. For large enough disturbances the flow distortion caused by symmetric wake unexpectedly becomes antisymmetric in spanwise direction. If the leading edge is too blunt the maximal distortion takes place immediately at the nose and no further amplification was observed. All these conditions and results are beyond the scope of Goldstein's theory.

14. SUBJECT TERMS	15. NUMBER OF PAGES
Receptivity, transition, stream disturbances	47
	16. PRICE CODE: A03

17. SECURITY CLASSIFICATION OF REPORT	18. SECURITY CLASSIFICATION OF THIS PAGE	19. SECURITY CLASSIFICATION OF ABSTRACT	20. LIMITATION OF ABSTRACT
unclassified	unclassified	unclassified	

NSN 7540-01-280-5500

Standard Form 298 (Rev. 2-89)
Prescribed by ANSI Std. Z39-18
298-102